Reply to the comments provided by the Anonymous Referee #1 on the manuscript amt-2020-27 entitled "Spectral Correction of turbulent energy damping on wind LiDAR measurements due to spatial averaging", by M. Puccioni and G. V. Iungo

The authors are greatly thankful to the Reviewer for the thorough review and insightful comments. Our replies are reported in the following. References to pages and lines are based on the revised marked-up manuscript.

General comment

- *The manuscript "Spectral correction of turbulent energy damping on wind LiDAR measurements due to range-gate averaging" by Puccioni and Iungo deals with the problem of spatial filtering by the probe volume of pulsed Doppler wind lidar instruments. This spatial filtering challenges the proper characterization of turbulence. Therefore, they propose an empirical transfer function, which under certain conditions, can be used to empirically correct the filtering effect. This transfer function is fitted to the ratio between the estimated power spectral density (PSD) of the along-beam velocity component and an empirical spectral model. This empirical model is based on the Blunt* model (Olesen *et al.,* 1984) *and is fitted to the low-frequency range of the estimated velocity spectrum. The solution proposed by Puccioni and Iungo is practical and simple, which is appreciated. The dataset is not novel but this is not so important here. In this regard, the paper is within the scope of AMT. The language is fluent but sometimes unprecise or unclear. While the conclusions of the paper support the proposed method and the overall content is clear…*

R: We thank the Reviewer for the positive feedback on our research strategy and the results achieved. It has been instrumental to leverage various LiDAR datasets, which have been collected by our group in collaboration with other colleagues, to prove the general applicability of the proposed model. Writing has been improved throughout the manuscript.

- *I have the impression that a significant portion of the manuscript is filling. The size of the manuscript could be reduced by 40 % without affecting its core message. The value of a paper is not defined by its length, fortunately. The filling is sometimes counter-productive as shown in section 6, where the authors use synthetic turbulence generation to work exclusively in the frequency domain: there is no need to generate any turbulent field in the time-domain if the calculations are conducted on the velocity spectra only. This section deals with an interesting topic, which is the dependency of the spatial averaging on the mean wind speed and the variance of the velocity component. However, unnecessary steps are used to reach the conclusion, which erode the analysis.*

R: We are research enthusiasts and very meticulous in the execution of our projects. If sometimes, unfortunately, we end up writing lengthy manuscripts is definitely not connected with the need of filling a document, which is clearly not needed considering the length of the text, rather prove the research assumptions and corroborate our results. We have significantly shortened the manuscript and sharpened its focus. Sect. 6 has been significantly revised, and only the part related to the variability of the energy damping with wind speed, standard deviation, and sampling height is kept.

- *The data processing is not always clear. Also, data are sometimes over-processed. The main fitting algorithm is likely applicable only if the spectral peak is not affected by spatial filtering. If the spectral peak is filtered out, the peak frequency will become "corrupted". This limitation is not clearly highlighted in the manuscript.*

R: We definitely agree with the Reviewer's comment and the mentioned constraint, namely ensuring that the spectral peak in not corrupted during the post-processing, has been always verified for our data analysis. In the revised version of the manuscript, we have highlighted the importance of verifying that the energy content in the proximity of the spectral peak is not altered by the post-processing procedure. In the manuscript at line 147, it is now reported: "If during the iterative process, k_{Th} achieves a value equal or smaller than that corresponding to the spectral peak, k_p, then the procedure is arrested and a warning is dispatched indicating that the correction procedure was not successful".

- *References to the existing scientific literature can be inaccurate or misleading. The number of self-citations in the manuscript is equal to almost one-third of the total number of references, which might be a little too high.*

R: As recommended by the Reviewer, we have significantly shortened our reference list.

Specific comments

Point 1

The term "range-gate averaging" may be criticized because the range does not necessarily refer to the probe volume length. I suggest using the term "spatial averaging" or "volume averaging" as a safe alternative.

R: During the preparation of this manuscript, we were skeptical in using the term spatial averaging because different spatial-averaging processes may occur when operating scanning wind LiDARs, such as by varying continuously the scanning head in the azimuthal direction for VAD and PPI scans, or the elevation angle for RHI scans. Throughout the manuscript, the smoothing process under investigation is now referred to as spatial averaging, consistently with previous works, e.g. Frehlich et al. (1998) and Sjöholm et al. (2009).

Point 2

The first paragraph of the introduction reviews previous turbulence measurements in the atmosphere by Doppler wind lidar instruments. The majority of these references is inadequate:

- *It is unclear how the work by Trukenmüller et al. (2004), Horányi et al. (2015) or Schepers et al. (2012) are related to Doppler Wind lidar measurements. I suggest removing these references.*
- *The works by Calhoun et al. (2006), Vanderwende et al. (2015) and El-Asha et al. (2017) are interesting but they are not about turbulence measurements. Their focus was on the mean wind speed only. I suggest removing these references.*
- *The reference to Grubišic et al. (2008) may not be appropriate because the lidars were not used to investigate turbulence characteristics. If the authors believe that a similar study must be included, the work by Spuler and Mayor (2005) might be more relevant. Note that Spuler and Mayor only collected snapshots of coherence structures, which may not be considered as "turbulence characterization" but rather "flow visualization".*

- *The reference to Fernando et al. (2019) may be replaced by the reference to Bodini et al. (2017) since the method used by Fernando et al. to study the turbulence dissipation rate is taken from Bodini et al.*
- *The reference to George and Yang (2012) may be removed because it is a review paper on vortices detection by various instruments. They did not focus on turbulence characterization and did not show any results from Doppler wind lidar measurements.*
- *Only self-references are used to illustrate turbulence measurements by lidars in the field of wind energy. In addition, the same results are sometimes cited multiple times because they are included in different similar papers. I recommend choosing only one of these papers and to not use self-references only.*

R: We have revised the mentioned references according with the comments of the Reviewer.

Point 3

Section 1: Some lines mentioning that the paper focuses on scanning pulsed Doppler wind lidar and not continuous-wave lidars or wind profilers may be necessary for the sake of clarity.

R: We definitely agree with this comment, indeed our discussion focuses completely on pulsed wind LiDARs. For instance, at line 45 it is reported: “A pulsed Doppler wind LiDAR, like those used for the present work…”.

Point 4

Line 27-28: The sentence “Turbulence statistics of the wind velocity field can be retrieved through fixed scans while providing a spectral characterization of the inertial sub-layer” is only partly true. If the probe volume is larger than 50 m, there exist situations where spatial filtering can affect the entire inertial subrange, preventing the detailed characterization of turbulence.

R: That sentence has been revised as (line 30): “Provided the use of a probe length, l, sufficiently small to probe the inertial sublayer at a height from the ground z, e.g. $l < 2\pi z$ according to Banerjee et al. (2015), turbulence statistics of the wind velocity field can be retrieved through fixed scans, while providing a spectral characterization of the inertial sub-layer (Iungo et al., 2013)”.

Point 5

Line 29: The reference to the detection of very large coherence structures is a little strange here because it does not imply the possibility to establish turbulence statistics from them. In particular, the experiment by Calaf et al. was done without knowing precisely the wind direction as they had no access to wind vanes or anemometers. Besides, the scientific literature contains many more examples of turbulence characteristics retrieved from fixed line-of-sight scans.

R: We thank the Reviewer for this comment. The reference to the paper Calaf et al. (2013) and the related text have been removed.

Point 6

Line 32: The reference to Mann et al. (2009) is only partly true: They actually estimated the auto and cross-spectral densities for the three velocity components, which is more advanced than the turbulent momentum flux.

R: The Reviewer is right. At line 35, it is now reported: “In Mann *et al.* (2009), auto- and cross-spectral densities for the three velocity components were estimated through multiple scanning-LiDAR measurements”.

Point 7

Line 34: A probe volume below 20 m is not so common for commercially available pulsed Doppler wind lidar. Maybe some comments can be written here.

R: Only LiDAR units for research on ABL turbulence may provide capabilities to perform measurements with very short-range gates, e.g. 20 m. At line 38, it is now reported: "… wind LiDARs tailored for investigations on atmospheric-turbulence currently provide probe volumes smaller than 20 m…".

Point 8

Line 42-43: The influence of the misalignment between the wind direction and laser beam could also be mentioned as an additional effect on the spatial filtering by the probe volume (see e.g. Held and Mann (2018)).

R: This is correct. Indeed, at line 130, it is reported: "… features of the low-pass filter and, thus, of the LiDAR measuring process, are functions of …relative angle between wind direction and azimuth angle of the laser beam …".

Point 9

Line 49: In Cheynet et al. (2017), the probe volume length was 75 m and the range gate length was 100 m. The probe length of 100 m mentioned in their study was used as an example to illustrate the spatial filtering.

R: At line 53, that statement is now revised as: "For single-point measurements performed with a Windcube 200S LiDAR and azimuthal angle of the laser beam set equal to the mean wind direction, a variance reduction of 8% was predicted for a gate length of 25 m, while it was increased up to 20% for a gate length of 100 m (Cheynet et al. , 2017)."

Point 10

In section 2, equation (1) is not necessary for the paper. Since the spatial filtering is a function of the wavenumber, using f (in Hertz) instead of n = f z/U is not desirable. Therefore, the study can be simplified by considering only equation 2.

R: We agree that providing both formulas might be redundant. The only equation with the reduced frequency, *n*, is now reported.

Point 11

The Kaimal model and Simiu-Scanlan models are particular cases of Equation 2. Note that in Kaimal et al. (1972), An = 105 and Bn = 33 but in Kaimal and Finnigan (1994), An = 102 and Bn = 33. Equation (2) with unspecified An and Bn values should be referred to as the blunt model (Olesen et al., 1984) instead of Kaimal model. The reference to ESDU is incorrect here. The ESDU standard is using a modified von Karman model, which has a form different from Equation 2. Therefore, I suggest removing the reference to ESDU.

R: We added in the manuscript that in Olsen *et al., 1984* the used spectral model is referred to as blunt model. However, even in that paper, it is reported that the spectral model was already used in Kaimal *et al.* 1972, for unstable conditions in Kaimal *et al.* 1976, Panofsky 1978, Højstrup 1981 and 1982, while for stable conditions in Kaimal 1973 and Caughey 1977. More recent papers refer to this spectral model as Kaimal model, see e.g. Risan *et al.* 2018, Worsnop *et al.* 2017 and even in the IEC standards for wind energy (International Electrotechnical Commission (2007) IEC 61400-1: Wind turbines—part 1: design requirements. 3rd edn). In the text at line 91, it is now reported: "The spectral model of Eq. 1 is typically referred to as blunt model (Olesen *et al*., 1984) or Kaimal model (Kaimal *et al*., 1972; IEC, 2007; Worsnop *et al*., 2017; Risan *et al*., 2018), and the parameter A is typically assumed equal to 105 (Kaimal *et al*., 1972), later revised to 102 (Kaimal & Finnigan, 1994), and B equal to 33."

Point 12

The algorithm in Figure 1 is interesting but also perfectible. It does not clearly show why the iterative procure is necessary and this should be explained in a pedagogical way. For example, it could be stated that there is no need to have an iterative procedure if f_{th0} is equal or lower than 0.01 Hz. There is an argument in favor of the iterative procedure that is not clearly stated in section 2: Choosing a value of f_{th0} too low will result in a poor fit of the velocity spectrum because the number of data points will be reduced. In addition, these points are associated with larger uncertainties than at higher frequencies. At the same time, if f_{th0} is larger than the cut-off frequency, the fitting will be significantly affected by the spatial filtering. There is also a potential limit for the application of this algorithm that was not clearly shown in the manuscript: the spectral correction may fail if the spectral peak is affected by the spatial filtering. Therefore, the proposed method might only be adequate for probe volume of 50 m or lower. That is an issue that deserves further discussion.

R: We have revised the flowchart of Fig. 1 according to the Reviewer's comments and added more details for the iterative process used for the estimation of k_{Th}. At line 137, it is now reported: "First, the pre-multiplied spectrum of the radial velocity projected in the horizontal mean wind direction is fitted with the spectral model of Eq. 1 only for wavenumbers smaller than $k_{Th,0} = 2\pi/l$. Indeed, we expect to observe significant spatial-averaging effects for turbulent length scales smaller than the probe length, l. For wavenumbers higher than the selected cut-off value, the ratio between the fitted Kaimal spectrum and the PSD of the LiDAR velocity, φ_*^2, is calculated to quantify the effect of the energy damping due to the LiDAR measuring process. Subsequently, the LiDAR-to-Kaimal ratio, φ_*^2, is fitted with Eq. 9 through a least-square algorithm to estimate the filter order, α, and provide an updated value for the cutoff wavenumber, k_{Th}. This process is iterated until convergence on the parameter k_{Th} is achieved (for this work, the convergence condition imposed is a variation of k_{Th}smaller than 1% of the previous value). If during the iterative process, k_{Th}achieves a value equal or smaller than that corresponding to the spectral peak, k_p, then the procedure is arrested and a warning is dispatched indicating that the correction procedure was not successful. This warning condition never occurred for all the data analyzed in this work. Furthermore, it should be considered that when k_{Th} achieves values close to k_p, the part of the velocity spectrum, Su, used for the fitting procedure with Eq. 1 can be so limited to jeopardize the accuracy of the fitting procedure.

Point 13

Equation 10: The spatial filtering is a function of the wavenumber rather than the frequency. Therefore, I think that fitting a modified version of Eq. 10, where the frequency is replaced by the wavenumber, may be more appropriate than the original version of Eq. 10.

R: As recommended by the Reviewer, the filter of Eq. 9, it is now expressed as a function of the wavenumber, k.

Point 14

Section 2: is the fitting algorithm a least-square fit?

R: That is correct. At line 142, it is now reported: "Subsequently, the LiDAR-to-Kaimal ratio, φ_*^2, is fitted with Eq. 9 through a least-square algorithm to estimate the filter order, α…"

Point 15

Line 145: Was the lidar azimuth set manually as equal to the mean wind direction or was it an automated procedure?

R: For the SLTEST and Celina datasets, the azimuth was set automatically by using the feedback scan modality provided in the software of the Streamline XR LiDAR manufactured by Halo Photonics. At line 174, it is now reported: "… the azimuth angle for the fixed scans was updated automatically at the end of each DBS or VAD scan through the feedback scan mode embedded in the LiDAR software and using the wind-direction value measured at height of 53 m".

Point 16

Line 148: Maybe it can be explained why the sampling frequency was varying between 0.5 Hz and 3.3 Hz?

R: We thank the Reviewer for this observation. The statement has been revised as follows (line 177): "To investigate possible variations of the averaging process related to the accumulation time, the sampling frequency of the fixed scans was varied between 0.5 Hz and 3.3 Hz, while the range gate was always set equal to 18 m".

Point 17

Figure 2: The topography is a little difficult to see. Maybe you can use a digital terrain model?

R: We do not aim to provide any specific information about the terrain topography, rather aerial views of the site.

Point 18

Line 163: Since the Obukhov length is calculated, I suggest replacing "static atmospheric stability" by "dynamic atmospheric stability" or simply "atmospheric stability".

R: For the classification of static and dynamic stability we refer to Sect. 5.5 "Stability Concepts" of the book "An Introduction to Boundary Layer Meteorology" by Ronald B. Stull. Static stability is typically connected to convection and it is governed by the Richardson number, while an example of dynamic instability is the generation of Kelvin-Helmholtz waves, which is a shear-driven instability. For the sake of simplicity, we refer now in the manuscript to atmospheric stability.

Point 19

Line 178: I do not understand the link between the sentence and the reference to Hutchins et al. (2012). Maybe this reference is not necessary?

R: In Hutchins et al. (2012), the authors used horizontal and vertical arrays of sonic anemometers. To investigate transverse gradients, only data with the 10-minute averaged wind direction within the range ±20° from the direction perpendicular to the horizontal array were considered. The same criterion is now used to reject data with large deviations of the wind direction from the azimuthal angle of the LiDAR.

Point 20

Lines 182-191: These lines could be summarized into a single sentence: "The second-order stationarity is assessed using a moving standard deviation with a window length of 5 min and zero overlapping". The reference to Liu et al is not adequate since they did not invent the concept of moving standard deviation. Besides, I would recommend using overlapping windows for a more robust assessment of the flow stationarity. In Matlab, the function "movstd" can be used for this purpose.

R: The non-stationary index (IST) is a well-established parameter to investigate the statistical stationarity of time-series, see e.g. Foken *et al.,* 2004. It is not a moving standard deviation, rather a quantification of the percentage variability of the variance over sub-periods of the signal with respect to the variance of the entire signal. It is mathematically different from the moving standard deviation, indeed in Eq. 13, CV is not the signal, rather the variance. In Liu *et al.,* 2017, the IST has been successfully used to select stationary velocity signals collected through sonic anemometers at a site very similar to those involved in this work; hence, it is very relevant for our work.

Point 21

The test of the second-order stationarity is a nice addition by the authors. I would also recommend a test for the first-order stationarity using a moving mean function.

R: This is an interesting suggestion; however, the standard deviation and turbulence intensity already provide information about the variability of the signal in time over the mean.

Point 22

Line 190: Is there any reason for choosing 40% for the maximal IST value?

R: In Foken et al. (2004) and Liu et al. (2017) a maximum IST of 30% was used. For our work, based on sensitivity analysis, we decided to increase the maximum IST to 40% to enable larger data availability without modifying noticeably the results of our analysis.

Point 23

Line 192: I am not sure I understand the "gradient-based" procedure to remove outliers. Maybe one sentence can be written to make it clearer?

R: More details have been added for the gradient-based filter (line 223): "Specifically, the partial derivative in time of the radial velocity is calculated through a second-order central finite-difference scheme. Velocity samples with absolute partial derivative larger than 15 times the respective median value calculated over the entire signal are marked as outliers and replaced through the inpaint_nans function available in Matlab (D'Errico, 2004). The used threshold value is selected based on a sensitivity analysis".

Point 24

Line 194: There is no official Matlab function "inpaint". However, there exists the function "inpaint_nans" by D'Errico (2004), which is well respected. Is this the function that you were using? If yes, a reference to D'Errico (2004) can be used.

R: The proper name of the function and respective reference are now reported in the manuscript.

Point 25

Eq. 17: This equation is only valid for the mean wind speed. If the variance is computed, substantial errors may arise (see eq. 2 in Sathe and Mann (2012b), which is also valid for a LOS scan mode). Some comments are expected here.

R: We are thankful to the Reviewer for bringing up this important comment. The along-beam (radial or LOS) velocity variance $\sigma_{V_r}^2$ can be related to the Reynolds stress components as (Eberhard et al., 1989):

$$\sigma_{V_r}^2 = \sigma_u^2 \cos^2 \Phi \cos^2(\theta - \theta_w) + \sigma_v^2 \cos^2 \Phi \sin^2(\theta - \theta_w) + \sigma_w^2 \sin^2 \Phi$$
$$+\sigma_{uv} \sin[2(\theta - \theta_w)] \sin^2 \Phi + \sigma_{uw} \cos(\theta - \theta_w) \sin 2\Phi + \sigma_{vw} \sin 2\Phi \sin(\theta - \theta_w),$$

where $\sigma_u^2, \sigma_v^2, \sigma_w^2$ are the variance of the streamwise, spanwise and vertical velocity components, respectively, and σ_{uv}, σ_{uw} and σ_{vw} are the shear Reynolds stresses. Considering the azimuth angle set in the mean wind direction ($\theta - \theta_w \approx 0$ ensured by constraining the dataset to wind direction variability to $\pm 20°$) and very small elevation angle, the previous equation can be approximated as:

$$\sigma_{V_r}^2 \approx \sigma_u^2 + \sigma_v^2(\theta - \theta_w)^2 + \sigma_w^2\Phi^2 + 2\sigma_{uv}(\theta - \theta_w)\Phi^2 + 2\sigma_{uw}(\theta - \theta_w)\Phi + 2\sigma_{vw}\Phi(\theta - \theta_w).$$

Even assuming all the Reynolds stresses with the same magnitude, it is evident that at the first order of approximation $\sigma_{V_r}^2 \approx \sigma_u^2$. Of course, this approximation is not valid for generic values of θ and Φ. At line 239, it is now added: "Furthermore, the variance of the radial velocity is the first-order approximation of the streamwise-velocity variance given the above-mentioned setup constraints (Eberhard et al., 1989, *Sathe and Mann, 2013*)."

Point 26

Line 228-229: The Savitzky-Golay smoothing filter was not designed by Balasubramaniam (2005) but by Savitzky and Golay (1964). I do not recommend using this filter to smooth the power spectral density (PSD) as it also distorts the low-frequency range of the spectrum. The goal should be to smooth only the high-frequency range, which includes enough data point. I advise to simply bin-average your data over bins that are uniformly spaced in the logarithmic space. This way, the fitting algorithm will also be improved. Alternatively, you can estimate the PSD using auto-regressive methods, which can produce fairly smooth PSD estimates if the random process of interest is broad-banded, which is the case here.

R: For our data analysis the smoothing with the Savitzky-Golay filter worked as good as bin-averaging, see the figure reported below where the original spectrum is initially high-pass filtered, then smoothed. This procedure does not affect the energy content of the spectral peak. For the smoothing, we used a polynomial function of the second order and the windows are calculated as $int[10(160k)^{0.5}]$, with k reported in 1/m, and *int* is rounding to the closest integer number (Balasubramaniam, 2005). At line 267, it is now reported: "For modeling purpose, the velocity spectra are then smoothed in the wavenumber domain following the Savitztky-Golay filter (Savitzky and Golay , 1964), by using a second-order polynomial function and windows with the width equal to *int*[10 (160 *k*)$^{0.5}$],where *k* is in m^{-1}and *int* is rounding to the closest integer number (Balasubramaniam , 2005)".

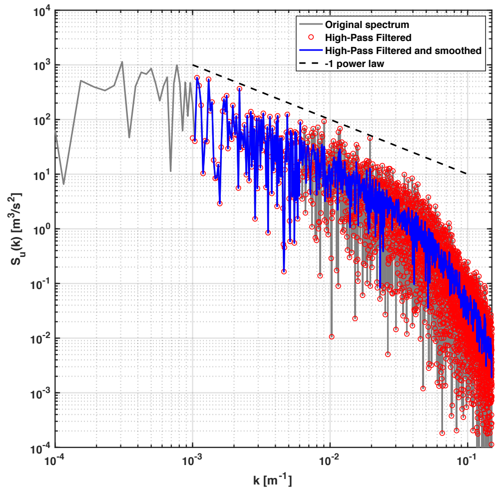

Point 27

The method to estimate the velocity spectrum should be explicitly stated. Since a fitting to the velocity spectrum is done, it is important to know if the PSD estimate is reliable or not. I do not recommend using the periodogram method. Alternatives approaches are the modified periodogram method (Welch, 1967) or the multitaper method (Thomson, 1982), both available in Matlab.

R: For the datasets collected at the Celina and SLTEST sites, the periodogram method has been substituted with the Welch spectrogram. However, very similar results are obtained with both methods. At line 329, it is now reported: "… the PSD of each velocity signal is then calculated with the pwelch function implemented in Matlab (Welch, 1967) without window overlapping and window width corresponding to k_{co}".

Point 28

Figure 5: The high-frequency range of the downsampled velocity spectrum seems to be slightly too high. This might be due to the presence of aliasing if the time series were downsampled without filtering. Decimating the original time series with a FIR filter and an order equal to at least 10 is recommended (cf. the Matlab function 'decimate'). This should lead to a better agreement between the velocity spectra of the lidar data and the sonic data.

R: We are thankful to the Reviewer for this comment and we agree that the down-sampled velocity spectrum might be affected by aliasing. We are now using the function "decimate" to downsample the data collected with the sonic anemometer. At line 285, it is reported: "The horizontal velocity retrieved from the sonic anemometer is first down-sampled with the sampling frequency of the LiDAR measurements, namely 2 Hz, using the Matlab function "decimate" with a finite-impulse response (FIR) low-pass filter with order equal to 10 (Weinstein, 1979)". Figure 5 has been revised accordingly.

Point 29

Line 263-264: The small difference between the difference range gate length is unlikely to explain the difference between the different filter functions. One possible reason for the discrepancies is the presence of measurement noise, which increases with the frequency and which is accounted for in the empirical filter function used in the manuscript but not modelled in eqs. 6-7.

R: The residual noise present in the LiDAR acquisition surely leads to an overestimation of the high-frequency spectrum. However, we think that it is unlikely that such a big overestimation performed by Eqs. 5 and 6 could be related to the sole measurement noise. At line 306, it is now reported: "A possible explanation for the poor performance of these deconvolution models could be the different probe length used for the XPIA campaign (*l*= 50 m) in contrast to *l*= 30 m used in the original study of that deconvolution model (Mann *et al*., 2009), and the presence of measurement noise in the data, which is not accounted for in the models of Eqs. 5 and 6".

Point 30

Figure 7 and the associated discussion do not seem to be a vital piece of information here. Firstly, the use of subsamples with an averaging time of 25 s could be criticized as it only includes a small portion of the turbulence spectrum. Therefore, the influence of the correction method on the variance estimate becomes exaggerated, which is not desirable in relation to algorithm validation. Secondly, only one time series is included, which limits the conclusions that can be drawn from this figure. It may be a careful choice to remove this figure and the corresponding paragraph.

R: This figure and related paragraph have been removed.

Point 31

Line 284-285: When applying a high-pass filter, the reader needs to know the exact value of the cut-off frequency, the order of the filter and what type of filter is applied. Therefore, mentioning a cut-off frequency of the order of 10^{-3} Hz is not sufficient. Velocity fluctuations around 1×10^{-3} Hz may still be representative of micro-scale turbulence. The use of the high-pass filter will increase the influence of the correction algorithm on the estimation of turbulence characteristics. This can be mentioned and/or quantified.

R: More details on the used high-pass filter are now reported in the manuscript. The filter cut-off frequency is selected to avoid modifications of the spectral content of the peak. An example of the application of the high-pass filter is reported in the figure of point 26. At line 249, it is now reported: "The LiDAR equivalent velocity, U_{eq}, is then high-pass filtered to remove low-frequency non-turbulent velocity fluctuations, using the following spectral transfer function:

$$G(k; S, k_{co}) = \frac{1 + \tanh\left[\beta \log\left(\frac{k}{k_{co}}\right)\right]}{2}$$

where k_{co} is the cutoff wavenumber, which should be smaller than k_p to avoid effects on the spectral peak. The parameter β is equal to 100 to generate a sufficiently sharp filter across the cutoff wavenumber, k_{co} (Hu *et al.,* 2019)".

Point 32

Figure 8 includes two subfigures that can be merged into a single one by using a 3-variable scatter plot, where the color of the markers reflects the variance. Nevertheless, I am not sure that figure 8 is vital to the paper.

R: We initially produced a similar figure to that mentioned by the Reviewer. However, it resulted to be more confusing without saving too much space in the manuscript. Therefore, we would keep this figure to provide a characterization of the background boundary-layer flows.

Point 33

Reference to Guala et al. (2006) is inadequate. They studied turbulence in pipe flows whereas the paper discusses turbulence in the atmospheric boundary layer. A more appropriate reference would be Counihan (1970).

R: That discussion has been removed.

Point 34

Figure 9 can be reduced to a single panel. I think showing the pre-multiplied spectrum fS_u *as a function of the wavenumber* k *is good enough.*

R: The inertial sub-range and the spectral correction is generally more evident through the power spectral density rather than through the pre-multiplied spectra. Plotting the spectra as a function of the reduced frequency, n, and wavenumber, k, is relevant for the implementation of the procedure. Indeed, more consistent values of the cut-off wavenumber are observed throughout the ASL height, which is not the case for n.

Point 35

Line 320: "selected dataset" is not specific enough. Maybe you can mention which data from which campaigns?

R: The sentence has been substituted with (line 369): "The proposed correction of the LiDAR measurements is now applied to all the datasets collected at Celina and SLTEST sites (see Table 2)".

Point 36

Figure 11 looks nice but it is not necessary to the paper. Firstly, because we cannot see a clear difference between the left and right panel and secondly because it does not bring particularly useful information. I suggest removing this figure for the sake of brevity.

R: This figure has been removed.

Point 37

Figure 12 is not necessary either to the paper. The textual description was already enough. I think this figure can be removed.

R: This figure has been removed.

Point 38

Line 330: I am not sure what you mean by a quasi-self-similar behavior. Figure 13 is showing (normalized) transfer functions. I think it may be wise to keep the description as simple as possible.

R: We mean that the empirical corrections practically collapse on the same curve, which corroborates that the filter proposed in Eq. 9 is actually a good model for the spatial averaging. At line 381, it is now reported: "… all the estimated transfer functions practically collapse on the same curve for measurements collected at different heights".

Point 39

Figure 15 could be replaced by a simple table showing the median value and the interquartile range, for example.

R: The results of Figure 15 are now reported in Table 3 and the discussion at lines 404-414 has been revised accordingly.

Point 40

Section 6 could be reformulated into one or two paragraphs. Firstly, the use of synthetic wind field is not useful here, as calculations are conducted in the frequency domain only. Secondly, the computation of the profiles of the mean wind speed and variance as well as the associated discussion is unnecessary. The right panel of Fig 17 is interesting but does not shows that the error ϵ could be expressed as a function of the mean wind speed and variance of the velocity only. I suggest shortening in section 6. It is possible to show the dependency of ε on the mean wind speed and the variance of the velocity as a contour map. Given a reference mean wind speed at a reference height, a logarithmic profile with and a given roughness length and the Kaimal spectrum, constructing such a map is straightforward. To change the mean wind speed parameter, you simply need to change the reference mean wind speed value. To change the variance of the along-wind component, you can simply change the roughness length.

R: We are greatly thankful to the Reviewer for this highly constructive comment. Sect. 6 has been significantly shortened and the variability of the spatial averaging with friction velocity, aerodynamic roughness length, and sampling height is now reported.

Point 41

The conclusion should be reformulated following the previous comments.

R: Conclusions have been revised accordingly to the Reviewer's comments.

Technical corrections

Point 1

Lines 1-3 (abstract): Maybe you should mention that you are talking about "pulsed" lidar systems. Continuous-wave Doppler wind lidars can measure the flow within a volume much lower than 20 m and a sampling frequency of several hundreds of Hertz.

R: In the abstract, it is now reported (line 1): "… pulsed wind LiDAR technology…".

Point 2

Line 2 (abstract): a sampling frequency of the order of 10 Hz is mentioned. Do you mean 1 Hz, as written in the manuscript?

R: In the manuscript, we mention sampling frequency higher than 1 Hz and LiDARs achieving sampling frequency around 10 Hz are now available.

Point 3

Line 3 (abstract): the expression "back-scattered laser beam" may not be correct. Do you mean "backscattered light" or "backscattered signal"?

R: It is now revised to back-scattered LiDAR signal.

Point 4

Lines 9 (abstract): I suggest replacing "estimated directly from the LiDAR measurement" by a more accurate term: "estimated directly from the power spectral densities of the along-beam velocity component".

R: This sentence has been revised accordingly.

Point 5

Line 34: The sentence "probe volumes, denoted as range gates" can be misunderstood by the reader and should be reformulated. The range gate length is different from the probe volume. For example, a range gate length shorter than the probe volume implies that the probe volumes are overlapping.

R: That's correct, the range gate is equal to the probe volume only for non-overlapping probe volumes, which is the case for all the datasets under investigation. The term range gate has been substituted with probe volume or length throughout the manuscript.

Point 6

Line 36: The syntax of the sentence "by means of a laser beam, which is back-scattered" is a little strange. I would write that the light is backscattered but not that the "laser beam" is backscattered.

R: At line 42, it is now reported: "… utilizing a laser beam, whose light is back-scattered…"

Point 7

Line 38: "from the Doppler shift on the back-scattered signal" should be "from the Doppler shift of the back-scattered signal"

R: Revised.

Point 8

Line 38: "like those used for the present work" should be "like the one used in the present work".

R: We used more than one LiDAR and this sentence is grammatically correct.

Point 9

The tilde symbol in Equation 10 and equation 11 may be explicitly defined for the sake of clarity.

R: At line 129, the following statement has been added: "The symbol $\tilde{\cdot}$ is used to differentiate the analytical model of the low-pass filter from its empirical estimate through the ratio between the fitted Kaimal spectrum and the PSD of the LiDAR velocity, φ_*^2".

Point 10

Line 156: "of the used LiDARs" may be written "of the LiDARs used" instead.

R: Corrected.

Point 11

Line 175-176: "For the SLTEST and Celina campaigns [...]through DBS or VAD scans" seems to be a repetition of the same information mentioned earlier in the manuscript. Maybe this sentence can be removed.

R: This sentence has been removed.

Point 12

Line 192: Consider replacing present tense by past tense when describing the data processing.

R: We typically use the present tense for post-processing and past tense for tasks related to the execution of the experiments and results/tasks from previous works.

Point 13
Line 251: The "spectrum of the lidar signal" should be replaced with "spectrum of the LOS velocity"
R: Corrected.

Point 14
Line 276: You may replace "linear regression analysis" by "comparison", which is much simpler.
R: We performed a linear regression, which has a clear mathematical definition to estimate, slope, bias, r-square value, etc.

Point 15
Line 287: The term "first and second-order statistics" can be replaced by "mean value and variance", which are the quantities you study in the paper.
R: Corrected.

Point 16
Line 307: The sentence "fitting of the LiDAR spectra" should be replaced with "fitting of the Blunt model to the along-beam velocity spectra".
R: Throughout the manuscript, we use "… fitting with the spectral model of Eq. 1".

Point 17
Line 324: "highest LiDAR gate" should be replaced by "highest LiDAR range gate" or "LiDAR range gate furthest from the instrument".
R: Revised.

Point 18
Line 336: " [...] always underestimate [...]" Do you mean "overestimate" ?
R: The analytical models underestimate, it means they should correct more to generate corrected spectra closer to those estimated through the spectral model.

Point 19
Figure 13: The term "convolution function" sounds strange. I would call it "transfer function" as it is the case in the field of signal processing.
R: Corrected.

Point 20
Line 359: Convolution in the time domain is multiplication in the frequency domain. Therefore, writing that the "synthetic velocity signal is convoluted in the frequency domain" is unclear. I think it may be simpler to write that the velocity spectrum is multiplied with the transfer function modelling the spatial averaging.
R: This part has been removed.

References

Balasubramaniam, B. J. (2005). Nature of turbulence in wall bounded flows. Ph.D. thesis of the University of Illinois at Urbana-Champaign Graduate College.

Banerjee, T., Katul, G. G., Salesky, S. T., & Chamecki, M. (2015). Revisiting the formulations for the longitudinal velocity variance in the unstable atmospheric surface layer. Quarterly Journal of the Royal Meteorological Society, 141(690), 1699–1711.

Bodini, N., Zardi, D., & Lundquist, J. K. (2017). Three-dimensional structure of wind turbine wakes as measured by scanning lidar. Atmospheric Measurement Techniques, 10(8).

Caughey, S. J. (1977). Boundary-layer turbulence spectra in stable conditions. Boundary-Layer Meteorology, 11(1), 3-14.

Cheynet, E., Jakobsen, J. B., Snæbjörnsson, J., Mann, J., Courtney, M., Lea, G., & Svardal, B. (2017). Measurements of surface-layer turbulence in awide norwegian fjord using synchronized long-range doppler wind lidars. Remote Sensing, 9(10), 1–26.

Counihan, J. (1970). Further measurements in a simulated atmospheric boundary layer. Atmospheric Environment (1967), 4(3), 259-275.

D'Errico, J. (2004). Inpaint nans. MATLAB Central File Exchange.

Eberhard, W. L., Cupp, R. E., & Healy, K. R. (1989). Doppler Lidar Measurement of Profiles of Turbulence and Momentum Flux. Journal of Atmospheric and Oceanic Technology, 6, 809-809-819.

Foken, T., Göockede, M., Mauder, M., Mahrt, L., Amiro, B., & Munger, W. (2004). Post-field data quality control. Handbook of micrometeorology, 181-208. Springer, Dordrecht.

Frehlich, R., Hannon, S. M., & Henderson, S. W. (1998). Coherent Doppler lidar measurements of wind field statistics. Boundary-Layer Meteorology, 86(2), 233–256.

Guala, M., Hommema, S. E., & Adrian, R. J. (2006). Large-scale and very-large-scale motions in turbulent pipe flow. Journal of Fluid Mechanics, 554, 521–542.

Held, D. P., & Mann, J. (2018). Comparison of Methods to Derive Radial Wind Speed from a LiDAR Doppler Spectrum. Atmospheric Measurement Techniques Discussion, (August), 1–11.

Højstrup, J. (1981). A simple model for the adjustment of velocity spectra in unstable conditions downstream of an abrupt change in roughness and heat flux. Boundary-Layer Meteorology, 21(3), 341-356.

Højstrup, J. (1982). Velocity spectra in the unstable planetary boundary layer. Journal of the Atmospheric Sciences, 39(10), 2239-2248.

Hu, R., Yang, X. I. A., & Zheng, X. (2019). Wall-attached and wall-detached eddies in wall-bounded turbulent flows. Journal of Fluid Mechanics, 885, A30-24.

Hutchins, N., Chauhan, K., Marusic, I., Monty, J., & Klewicki, J. (2012). Towards reconciling the large-scale structure of turbulent boundary layers in the atmosphere and laboratory. Boundary-Layer Meteorology, 145(2), 273–306.

International Electrotechnical Commission (2007) IEC 61400-1: Wind turbines—part 1: design requirements. 3rd edn.

Iungo, Giacomo Valerio, Yu-Ting Wu, and Fernando Porté-Agel (2013). Field measurements of wind turbine wakes with lidars. Journal of Atmospheric and Oceanic Technology 30(2), 274-287.

Liu, H. Y., Bo, T. L., & Liang, Y. R. (2017). The variation of large-scale structure inclination angles in high Reynolds number atmospheric surface layers. Physics of Fluids, 29(3).

Kaimal, J. C., Wyngaard, J. C., Izumi, Y., & Coté, O. R. (1972). Spectral characteristics of surface-layer turbulence. Quarterly Journal of the Royal Meteorological Society, 98(417), 563–589.

Kaimal, J. C. (1973). Turbulenece spectra, length scales and structure parameters in the stable surface layer. Boundary-Layer Meteorology, 4(1–4), 289–309.

Kaimal, J. C., Wyngaard, J. C., Haugen, D. A., Coté, O. R., Izumi, Y., Caughey, S. J., & Readings, C. J. (1976). Turbulence structure in the convective boundary layer. Journal of the Atmospheric Sciences, 33(11), 2152-2169.

Kaimal, J. C., & Finnigan, J. J. (1994). *Atmospheric boundary layer flows: their structure and measurement*. Oxford university press.

Mann, J., Cariou, J. P., Courtney, M. S., Parmentier, R., Mikkelsen, T., Wagner, R., Enevoldsen, K. (2009). Comparison of 3D turbulence measurements using three staring wind lidars and a sonic anemometer. Meteorologische Zeitschrift, 18(2), 135–140.

Marusic, I., Monty, J., Hultmark, M., & Smits, A. J. (2013). On the logarithmic region in wall turbulence. Journal of Fluid Mechanics, 716(2), R3-1 R3-11.

Monin, A. S., & Obukhov, A. M. (1954). Basic laws of turbulent mixing in the surface layer of the atmosphere. Contrib. Geophys. Inst. Acad. Sci. USSR, 24(151), 163–187.

Panofsky, H. A. (1978). Matching in the convective planetary boundary layer. Journal of the Atmospheric Sciences, 35(2), 272-276.

Risan, A., Lund, J. A., Chang, C. Y., & Sætran, L. (2018). Wind in Complex Terrain-Lidar measurements for evaluation of CFD simulations. Remote Sensing, 10(1), 1–18.

Sathe, A. and Mann, J.: A review of turbulence measurements using ground-based wind lidars, Atmos. Meas. Tech., 6, 3147-3167, https://doi.org/10.5194/amt-6-3147-2013, 2013.

Savitzky, A., & Golay, M. J. (1964). Smoothing and differentiation of data by simplified least squares procedures. Analytical chemistry, 36(8), 1627-1639.

Sjöholm, M., Mikkelsen, T., Mann, J., Enevoldsen, K., & Courtney, M. (2009). Spatial averaging-effects on turbulence measured by a continuous-wave coherent lidar. Meteorologische Zeitschrift, 18(3), 281–287.

Stull, R. B. (1988). An introduction to boundary layer meteorology. Atmospheric sciences.

Taylor, G. I. (1938). The spectrum of turbulence. Proceedings of the Royal Society of London. Series A-Mathematical and Physical Sciences, 164(919), 476-490.

Thomson, D. J. (1982). Spectrum estimation and harmonic analysis. Proceedings of the IEEE, 70(9), 1055-1096

Weinstein, C. J. (1979). Programs for digital signal processing. IEEE.

Welch, P. (1967). The use of fast Fourier transform for the estimation of power spectra: a method based on time averaging over short, modified periodograms. IEEE Transactions on audio and electroacoustics, 15(2), 70-73.

Worsnop, R. P., Bryan, G. H., Lundquist, J. K., & Zhang, J. A. (2017). Using large-eddy simulations to define spectral and coherence characteristics of the hurricane boundary layer for wind-energy applications. *Boundary-Layer Meteorology*, *165*(1), 55-86.

Reply to the comments provided by Anonymous Referee #3 on the manuscript amt-2020-27 entitled "Spectral Correction of turbulent energy damping on wind LiDAR measurements due to range-gate averaging", by M. Puccioni and G. V. Iungo

The authors are greatly thankful to the Reviewer for the thorough review and insightful comments. Our replies are reported in the following. References to pages and lines correspond to those of the latest marked-up manuscript.

General comments

This manuscript proposes a new method to correct turbulence measurements by Doppler lidar for low-pass filtering due to spatial averaging along the laser path. This is done by a combination of empirical transfer functions with classical Kaimal model spectra. The new approach is similar to commonly-used spectral correction methods for turbulence measurements by sonic anemometers (e.g. Moore, 1986), but at least to my knowledge, this has not be done before in this way for Doppler lidar measurements. The article is generally well written, perhaps a bit lengthy; the structure is clear and the figures are instructive, and the conclusions are drawn correctly. Nevertheless, I have two main comments, which are somewhat related:

R: We thank the Reviewer for the positive comments on our research strategy and the results achieved.

Comments

1) Because Kaimal model spectra are based on surface-layer scaling, the proposed correction is only applicable in the surface layer (on the order of 100 m). This important restriction should be made very clear in the manuscript, because modern Doppler lidars often cover the entire boundary layer (on the order of 1000 m), and do not cover the first ca. 50 m. The authors need to clarify this when describing the scope of this study in the introduction section and also in the discussion and conclusion sections.

R: The authors are thankful to the Referee for this observation. We have highlighted throughout the manuscript that the proposed method only applies to LiDAR data collected within the surface layer. In the Abstract, L21: "On the other hand, the proposed method assumes that surface-layer similarity holds". In the Introduction, L 87, it is now reported: "It is noteworthy that this method leverages surface layer similarity (Stull, 1988), thus it can only be applied for wind LiDAR measurements collected within the ASL". At L 182: "On the other hand, the proposed procedure leverages the surface-layer similarity for the Kaimal spectral model for the streamwise model and, thus, it can only be applied for wind LiDAR measurements collected within the ASL". In the Conclusions, L 556: "It is noteworthy that the Kaimal spectral model leverages surface layer similarity and, thus, the proposed method can only be used for LiDAR measurements collected within the atmospheric surface layer (ASL)".

2) The literature review in the introduction section is incomplete. Particularly, one important reference is missing (Brugger et al., 2016), which has the same objective of proposing a spectral correction method for Doppler lidars to compensate for spatial averaging along the laser path. However, the underlying approach is very different (Frehlich and Cornman, 2002), which is based on a von Kármán turbulence model. This has the advantage that it is independent of stratification or the driving mechanism of turbulence. The authors need to explain what the differences between *the two approaches are, theoretical and practical, disadvantages and advantages, and they also need to justify why they propose this new method. This affects the introduction and also the discussion and conclusion sections.*

R: The authors are thankful to the Referee for this comment. The paper Brugger et al. (2016) is now reviewed in the Introduction. Furthermore, this method is compared to the proposed method and other two existing methods for one LiDAR dataset in the new Fig. 12. The advantages/disadvantages of the new method compared to existing methods are now better highlighted throughout the manuscript. In the Abstract, L19, it is now reported: "The method proposed for the correction of the second-order turbulent statistics of wind-velocity LiDAR-data is a compelling alternative to existing methods because it does not require any input related to the technical specifications of the used LiDAR system, such as the energy distribution over the laser pulse and LiDAR probe length. On the other hand, the proposed method assumes that surface-layer similarity holds". In the Introduction, L69: "Another method for spatial-averaging correction of wind LiDAR measurements was proposed in Brugger et al. (2016). By assuming a linear averaging over each range gate and a Gaussian shape of the energy along the laser pulse, this method estimates the corrected velocity variance and the outer scale of turbulence by leveraging the von Kármán model of the second-order structure function for the streamwise velocity (Von Kármán , 1948). The spatial averaging is included directly in the calculation of the structure function, following the work by Frehlich et al. (1998). In Brugger et al. (2016), compelling results were achieved comparing corrected LiDAR data with simultaneous and co-located data collected with an ultrasonic anemometer. However, these authors noticed residual systematic errors in the LiDAR corrected data, which might be related to the assumptions of the laser-pulse shape, the linear averaging process, or the von Kármán model of the structure function, which was originally formulated for isotropic neutrally-stratified turbulence (Von Kármán , 1948)". At L82: "In contrast to the above-mentioned methods for the correction of the streamwise velocity variance for LiDAR spatial averaging (Mann et al. , 2009; Sjöholm et al. , 2009; Brugger et al. , 2016), the correction method proposed in this paper does not require any a-priori information about the technical specifications of the used LiDAR systems, such as probe length or shape of the laser pulse. The proposed method allows us to correct the second-order statistics of the streamwise velocity from spatial averaging by inverting the effects of a low-pass filter, whose characteristics are directly determined from the power spectral density (PSD) of the LiDAR measurements. It is noteworthy that this method leverages surface layer similarity (Stull, 1988), thus it can only be applied for wind LiDAR measurements collected within the ASL". L 178: "It is noteworthy that in contrast to existing models using pre-defined functions to correct the energy damping of the velocity fluctuations, see e.g. Eqs. 5 and 6 (Sjöholm et al. , 2009; Brugger et al. , 2016; Cheynet et al. , 2017), which require information about the LiDAR probe length and the energy distribution over a pulse, the proposed procedure calculates the characteristics of the damping on the LiDAR velocity signals directly from the experimental data, which leads, as it will be shown in the following, to enhanced accuracy in the correction of the LiDAR velocity spectra. On the other hand, the proposed procedure leverages the surface-layer similarity for the Kaimal spectral model for the streamwise model and, thus, it can only be applied for wind LiDAR measurements collected within the ASL". At L 429: "For the SLTEST dataset (see Table 2), the correction of the velocity variance obtained with the proposed method (red marker in Fig. 12a) is compared with those obtained from Eq. 5 (dark green symbols), Eq. 6 (light green marker) and the method of Brugger et al. (2016) (blue marker). For the latter, a probe length of 18 m and a Full-Width Half-Maximum (FWHM) of the laser pulse for the Streamline XR Doppler LiDAR equal to 35 m are used (Risan et al. , 2018). Consistently with the spectra of Fig. 10, the correction methods of Eqs. 6 and 5 under-estimate the effects of spatial averaging of the streamwise velocity variance and they do not allow the complete recovery of the -5/3 slope of the inertial subrange. The correction based on the structure function proposed by Brugger et al. (2016) leads to a variance distribution larger than what is estimated by the new method based on the Kaimal spectral model, yet with percentage correction in the same order of magnitude (Fig. 12b)". New Fig. 12

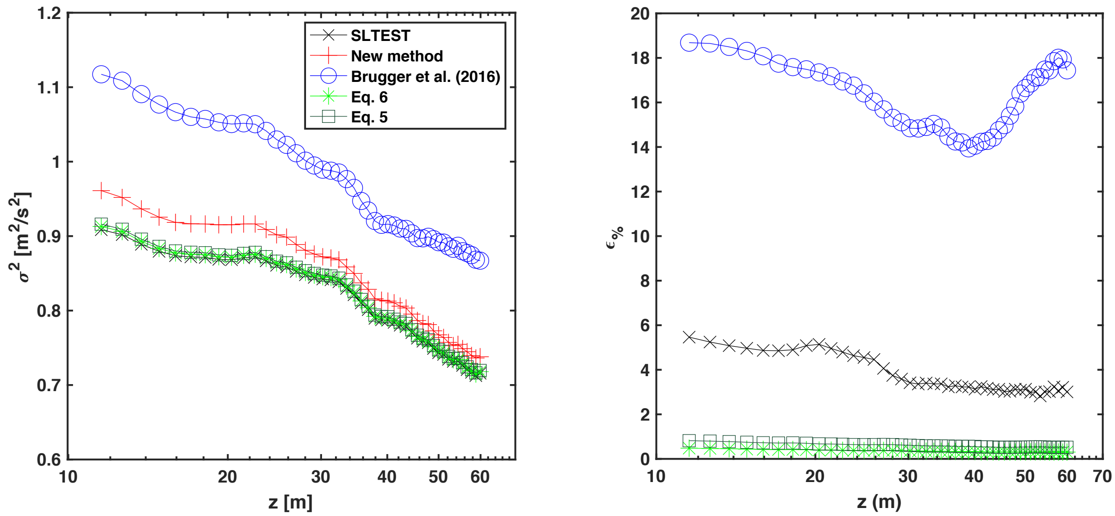

Figure 12. Correction of the streamwise velocity variance with different methods for the SLTEST dataset: (a) streamwise velocity variance; (b) percentage correction of the velocity variance, ε%. The marker colors are black for the raw LiDAR data, red for the proposed method, light green for Eq. 6, dark green for Eq. 5, and blue for the method proposed by Brugger et al. (2016).

In the Conclusions, L 543: "Existing methods propose to correct the effects of spatial averaging on LiDAR measurements using as input technical specifications of the used LiDAR systems, such as probe length and pulse energy distribution, which might not 545 be available and, thus often approximated with analytical functions". L 556: "It is noteworthy that the Kaimal spectral model leverages surface layer similarity and, thus, the proposed method can only be used for LiDAR measurements collected within the atmospheric surface layer (ASL). Specifically for this work, we performed fixed scans with low elevation angle (less than 10°) and azimuth angle equal to the mean wind direction to achieve good accuracy in the measurements of the streamwise velocity component, high vertical resolution (≈ 1m), measurements up to the ASL height, and high sampling frequency (between 1 and 3.3 Hz)". At L 564: "The compelling results obtained for the correction of the second-order statistics of LiDAR data corroborate the advantage of applying the proposed method, which does not require as input any information of the LiDAR system used, such as probe length and energy distribution over the laser pulse. In contrast to existing methods for correction of LiDAR spatial averaging, all the method parameters are directly estimated from the collected LiDAR data. However, the proposed method can only be applied for LiDAR data collected within the ASL".

Spectral correction of turbulent energy damping on wind LiDAR measurements due to ~~range-gate~~ spatial averaging

Matteo Puccioni and Giacomo Valerio Iungo

Wind Fluids and Experiments (WindFluX) Laboratory, Mechanical Engineering Department, The University of Texas at Dallas, 800 W Campbell Rd, 75080 Richardson, Texas, USA

Correspondence: Giacomo Valerio Iungo (valerio.iungo@utdallas.edu)

Abstract. Continuous advancements in pulsed wind LiDAR technology have enabled compelling wind turbulence measurements within the atmospheric boundary layer with ~~range gates~~ probe lengths shorter than 20 m and sampling frequency of the order of 10 Hz. However, estimates of the radial velocity from the back-scattered ~~laser beam~~ LiDAR signal are inevitably affected by an averaging process within each ~~range gate~~ probe volume, generally modeled as a convolution between the true velocity projected along the LiDAR line-of-sight and an unknown weighting function representing the energy distribution of the laser pulse along the ~~range gate~~ probe length. As a result, the spectral energy of the turbulent velocity fluctuations is damped within the inertial sub-range, thus not allowing to take advantage of the achieved spatio-temporal resolution of the LiDAR technology. We propose to correct ~~this~~ the turbulent energy damping on the LiDAR measurements by reversing the effect of a low-pass filter, which can be estimated directly from the ~~LiDAR measurements~~ power spectral density of the along-beam velocity component. LiDAR data acquired from three different field campaigns are analyzed to describe the proposed technique, investigate the variability of the filter parameters and, for one dataset, assess the corrected velocity variance against sonic anemometer data. It is found that the order of the low-pass filter used for modeling the energy damping on the LiDAR velocity measurements has negligible effects on the correction of the second-order statistics of the wind velocity. In contrast, the cutoff ~~frequency~~ wavenumber plays a significant role in spectral correction encompassing the smoothing effects connected with the LiDAR ~~gate~~ probe length. Furthermore, ~~the underestimation of the turbulence intensity modeled through the proposed filter is found to have a more pronounced effect for velocity acquisitions closer to the ground~~ the variability of the spatial averaging on wind LiDAR measurements is investigated for different wind speed, turbulence intensity, and sampling height. The results confirm that the effects of spatial averaging are enhanced with decreasing wind speed, smaller integral length scale and, thus, for smaller sampling height. The method proposed for the correction of the second-order turbulent statistics of wind-velocity LiDAR-data is a compelling alternative to existing methods because it does not require any input related to the technical specifications of the used LiDAR system, such as the energy distribution over the laser pulse and LiDAR probe length. On the other hand, the proposed method assumes that surface-layer similarity holds.

1 Introduction

Over the last decades, wind Doppler Light Detection and Ranging (LiDAR) technology has provided compelling features to perform wind turbulence measurements within the atmospheric boundary layer (ABL) for different scientific and industrial pursuits, such as air quality, meteorology (Spuler and Mayor , 2005; Emeis et al. , 2007; Bodini et al. , 2017), aeronautic transportation, and wind energy (Frehlich and Kelley , 2008; Zhan et al. , 2019). In the context of ABL turbulence, scanning Doppler wind LiDARs were assessed against other measurement techniques, such as sonic anemometers and scanning Doppler wind radars, during the eXperimental Planetary boundary layer Instrumentation Assessment (XPIA) campaign (Lundquist et al. , 2017; Debnath et al. , 2017a, b; Choukulkar et al. , 2017; Debnath , 2018).

Different scanning strategies can be designed to characterize different properties of the ABL velocity field through LiDAR measurements (Sathe and Mann , 2013), while the highest spectral resolution is achievable by maximizing the sampling frequency and measuring over a fixed line-of-sight (LOS). Provided the use of a probe length, l, sufficiently small to perform wind measurements within the inertial sub-layer, e.g. at a height from the ground, z, with $l < 2\pi z$ (Banerjee et al. , 2015), turbulence statistics of the wind velocity field can be retrieved through fixed scans while providing a spectral characterization of the inertial sub-layer (Iungo et al. , 2013) ~~and very large coherent structures present within the ABL~~. 3D fixed-point measurements can be performed by retrieving the radial velocity measured simultaneously by three or more LiDARs intersecting at a fixed position (Mikkelsen et al. , 2008; Carbajo et al. , 2014). In Mann et al. (2009), auto- and cross-spectral densities for the three velocity components were estimated through multiple scanning-LiDAR measurements. ~~Other turbulence statistics can also be evaluated through multiple scanning LiDARs, such as turbulent momentum fluxes (Mann et al. , 2009)~~

Besides the easier deployment compared to the installation of classical meteorological towers, wind LiDARs tailored for investigations on atmospheric-turbulence currently provide probe volumes ~~, denoted as range gates,~~ smaller than 20 m along the direction of the laser beam and sampling frequency higher than 1 Hz, which are welcomed features for studies on ABL turbulence.

A Doppler wind LiDAR allows probing the atmospheric wind field utilizing a laser beam, ~~which~~ whose light is back-scattered in the atmosphere due to the presence of particulates suspended in the ABL. The velocity component along the laser-beam direction, denoted as radial or LOS velocity, is evaluated from the Doppler shift ~~on~~ of the back-scattered signal. A pulsed Doppler wind LiDAR, like those used for the present work, emits laser pulses to perform quasi-simultaneous wind measurements at multiple distances from the LiDAR as the pulses travel in the atmosphere. The wind measurements performed over each ~~range gate~~ probe volume can be considered as the convolution of the actual wind velocity field projected along the laser-beam direction with a weighting function representing the radial distribution of the energy associated with each laser pulse. Therefore, LiDAR measurements can be considered as the result of low-pass filtering of the actual velocity field, where the characteristics of the low-pass filter are functions of the energy distribution of the laser pulse over the ~~range gate~~ probe volume, probe length ~~of the range gate~~, and accumulation time (Frehlich et al. , 1998; Sjöholm et al. , 2009; Held and Mann , 2018).

A reduced variance of the wind velocity is generally measured with a Doppler wind LiDAR compared with that measured through a sonic anemometer due to the laser-pulse averaging and different size of the measurement volume. For single-point measurements performed with a Windcube 200S LiDAR and azimuth angle of the laser beam set equal to the mean wind direction, a variance reduction of 8% was ~~quantified for a gate length of 25 m, while it increased up to 20% for a probe length of 100 m~~ predicted for a gate length of 25 m, while it was increased up to 20% for a gate length of 100 m (Cheynet et al. , 2017).

Attenuation of the measured turbulent kinetic energy due to the averaging over each probe volume can be corrected through a spectral transfer function introduced in Mann et al. (2009). For fixed scans, by leveraging the Taylor's frozen-turbulence hypothesis (Taylor , 1938; Panofsky and Dutton , 1984), the velocity energy spectrum is recovered through the deconvolution of the radial velocity with the weighting function representing the energy of the laser pulse. The critical part of this correction method consists of the empirical definition of the weighting function and its representative length scale (Banakh and Werner , 2005; Lindelöw , 2008; Mann et al. , 2009). As it will be shown in this paper, corrections performed through this deconvolution procedure often do not provide a satisfactory accuracy for wind turbulence measurements.

Another method for spatial-averaging correction of wind LiDAR measurements was proposed in Brugger et al. (2016). By assuming a linear averaging over each range gate and a Gaussian shape of the energy along the laser pulse, this method estimates the corrected velocity variance and the outer scale of turbulence by leveraging the von Kármán model of the second-order structure function for the streamwise velocity (Von Kármán , 1948). The spatial averaging is included directly in the calculation of the structure function, following the work by Frehlich et al. (1998). In Brugger et al. (2016), compelling results were achieved comparing corrected LiDAR data with simultaneous and co-located data collected with an ultrasonic anemometer. However, these authors noticed residual systematic errors in the LiDAR corrected data, which might be related to the assumptions of the laser-pulse shape, the linear averaging process, or the von Kármán model of the structure function, which was originally formulated for isotropic neutrally-stratified turbulence (Von Kármán , 1948).

In this work, a semi-empirical procedure is proposed to correct the damping of turbulent kinetic energy associated with wavelengths comparable to the LiDAR ~~range gate~~ probe length for turbulent velocity measurements collected within the atmospheric surface layer (ASL), which is defined as the lower portion of the ABL where momentum and thermal fluxes are assumed to be constant (Stull , 1988). The ASL height can be quantified through the analysis of the turbulent fluxes or the variance of the streamwise velocity as a function of height (Gryning et al. , 2016). In contrast to the above-mentioned methods for the correction of the streamwise velocity variance for LiDAR spatial averaging (Mann et al. , 2009; Sjöholm et al. , 2009; Brugger et al. , 2016), the correction method proposed in this paper does not require any a-priori information about the technical specifications of the used LiDAR systems, such as probe length or shape of the laser pulse. The proposed method allows to correct the second-order statistics of the streamwise velocity from spatial averaging by inverting the effects of a low-pass filter, whose characteristics are directly determined from the power spectral density (PSD) of the LiDAR measurements. It is noteworthy that this method leverages surface layer similarity (Stull , 1988), thus it can only be applied for wind LiDAR measurements collected within the ASL.

The remainder of this paper is organized as follows: the theoretical aspects of the correction procedure are discussed in §2, while in §3 the experimental campaigns performed to collect the various LiDAR datasets are described. In §4, an assessment of the proposed correction procedure is performed against sonic anemometry, while in §5 the correction procedure is tested for various LiDAR datasets. In §6, the spatial-averaging effects are investigated by varying the friction velocity, aerodynamic roughness length, and sampling height, thus for different mean wind speed and standard deviation ~~the relative importance of each low-pass filter's parameter is explored, first for a single synthetically-generated turbulence spectrum and then for a vertical array of them~~. Finally, concluding remarks are reported in §7.

2 Correction procedure for the LiDAR velocity spectra

Surface-layer scaling is typically used for spectral models of the wind speed assuming that the velocity integral length-scale is proportional to the height from the ground, z, and the Reynolds stresses can be normalized with the square of the friction velocity, u_τ.~~In this work, S_u is the PSD of the streamwise velocity and A_f and B_f are parameters estimated through best-fitting of the pre-multiplied energy spectra of the LiDAR velocity signals with Eq.~~1. ~~The term ϕ_ϵ (≥ 1) represents a dimensionless dissipation for non-neutral atmospheric stability regimes, with ϕ_ϵ equal to 1 for neutrally-stratified surface-layer flows~~ (Kaimal et al. , 1972).~~For this work, we only consider near-neutral atmospheric conditions and slight variations connected with atmospheric stability are embedded in the coefficient A_f of Eq.~~ 1. A classical approach to model the power spectral density of the streamwise velocity, S_u, is the following:

$$\frac{f\,S_u(f)}{u_\tau^2\,\phi_\epsilon} = \frac{A\,n}{(1+B\,n)^{5/3}}, \tag{1}$$

where f is frequency, $n = fz/U$ is the reduced frequency, U is the mean advection velocity, and A and B are parameters estimated through the best-fitting of the pre-multiplied energy spectra of the LiDAR velocity signals with Eq. 1. The term ϕ_ϵ (≥ 1) represents a dimensionless dissipation for non-neutral atmospheric stability regimes, with ϕ_ϵ equal to 1 for neutrally-stratified surface-layer flows (Kaimal et al. , 1972). For this work, we only consider near-neutral atmospheric conditions and slight variations connected with atmospheric stability are embedded in the coefficient A. ~~The wind velocity spectra can also be modeled as a function of the non-dimensional frequency $n = fz/U$ (U is the local average horizontal wind speed), as follows:~~ The spectral model of Eq. 1 is typically referred to as blunt model (Olesen et al. , 1984) or Kaimal model (Kaimal et al. , 1972; IEC , 2007; Worsnop et al. , 2017; Risan et al. , 2018), and the parameter A is typically assumed equal to 105 (Kaimal et al. , 1972), later revised to 102 (Kaimal and Finnigan , 1994), and B equal to 33. It is noteworthy that within the inertial sub-layer, the pre-multiplied spectra scale as $n^{-2/3}$, while the maximum value occurs for a reduced frequency equal to $1.5/B$, which corresponds to the wavenumber $k_p = 3\pi/(B\,z)$ ~~(non-dimensional frequency of $1.5/B_n$)~~.

Considering the Cartesian reference frame, (x_1, x_2, x_3), where the coordinates are aligned with streamwise, transverse, and vertical directions, respectively, the wind speed measured by a pulsed Doppler wind LiDAR can be modeled as the convolution between the projection of the wind velocity $\mathbf{u} = (u_1, u_2, u_3)$ along the laser-beam direction, $\mathbf{n} = (n_1, n_2, n_3)$, with a weighting function, ϕ, representing the energy distribution of the laser pulse within a ~~range gate~~ probe volume (Sjöholm et al. , 2009;

Mann et al. , 2009; Cheynet et al. , 2017):

$$v_r(x) = \int_{-l/2}^{l/2} \phi(s)\,\mathbf{u}(s\mathbf{n}+x)\cdot\mathbf{n}ds, \tag{2}$$

where v_r is the radial or line-of-sight velocity measured along the laser-beam direction, $\mathbf{n}$, at a radial distance x from the LiDAR. The probe length ~~of the range gate~~ is l, while s is the radial position within the considered ~~gate~~ probe volume. The weighting function, ϕ, is normalized to unit integral. If the Doppler frequency is determined as the first moment of the signal PSD with the background subtracted appropriately, then the weighting function can be expressed as (Banakh and Werner , 2005; Mann et al. , 2009; Cheynet et al. , 2017):

$$\phi_1(s) = \frac{l-|s|}{l^2} \tag{3}$$

For the LiDAR Windcube 200S, the following weighting function can also be used (Lindelöw , 2008; Mann et al. , 2009):

$$\phi_2(s) = \frac{3(l-|s|)^2}{2l^3} \tag{4}$$

In the spectral domain, the Fourier transform of Eq. (3) is:

$$\varphi_1 = \frac{\sin^2(0.5kl)}{(0.5kl)^2}, \tag{5}$$

while for Eq. 4 is:

$$\varphi_2 = \frac{6}{(kl)^2}\cdot\left[1-\frac{\sin(kl)}{kl}\right], \tag{6}$$

where $k = 2\pi f/U$ is the wavenumber evaluated through the Taylor's frozen-turbulence hypothesis (Taylor , 1938). As shown in Mann et al. (2009), the measured velocity spectrum, S_L, can be modeled as:

$$S_L(k_1) = n_i n_j \int_{-\infty}^{+\infty}\int_{-\infty}^{+\infty} |\varphi(\mathbf{k}\cdot\mathbf{n})|^2 \Phi_{ij}(\mathbf{k}) dk_2 dk_3, \tag{7}$$

where: $\mathbf{k} = (k_1,k_2,k_3)$ is the wavenumber vector and summation over repeated indices is assumed. In Eq. 7 , $\Phi_{ij}(\mathbf{k})$ is the spectral tensor obtained as Fourier transform of the Reynolds stress tensor and $\varphi(\mathbf{k}\cdot\mathbf{n})$ is the Fourier transform of the convolution function. When the laser beam stares along the mean wind direction with a relatively low elevation angle, namely with $\mathbf{n} \approx (1,0,0)$, the PSD of the radial velocity, S_L, is equal to the product between the spectrum of the actual radial velocity, $\hat{S}_L(k_1)$, and the square of the Fourier transform of the weighting function, $\varphi(k_1)$:

$$S_L(k_1) = \int_{-\infty}^{+\infty}\int_{-\infty}^{+\infty} |\varphi(k_1)|^2 \Phi_{ij}(\mathbf{k}) dk_2 dk_3 = |\varphi(k_1)|^2 \hat{S}_L(k_1). \tag{8}$$

Equation 8 shows that the spectrum of the measured radial velocity, S_L, is equal to the true velocity spectrum, $\hat{S}_L$, low-pass filtered with a certain transfer function. In this work, the latter is modeled as:

$$\cancel{|\tilde{\varphi}|^2(f) = \left[1+\left(\frac{f}{f_{Th}}\right)^{\alpha}\right]^{-1}},$$

$$|\tilde{\varphi}|^2(k) = \left[1+\left(\frac{k}{k_{Th}}\right)^{\alpha}\right]^{-1}, \tag{9}$$

where α and $\cancel{f_{Th}}$ k_{Th} represent the order and cutoff ~~frequency~~ wavenumber, respectively, of a low-pass filter (Ogata , 2010). The symbol $\tilde{\cdot}$ is used to differentiate the analytical model of the low-pass filter from its empirical estimate through the ratio between the fitted Kaimal spectrum and the PSD of the LiDAR velocity, φ_*^2. These features of the low-pass filter and, thus, of the LiDAR measuring process, are functions of the LiDAR ~~range gate~~ probe length, the elevation angle of the laser beam, the relative angle between wind direction and azimuth angle of the laser beam, accumulation time, and characteristics of the laser pulse. Therefore, it is highly challenging to predict these parameters a priori, while it ~~seems more efficient~~ is advisable to estimate α and $\cancel{f_{Th}}$ k_{Th} directly from the specific LiDAR data under analysis. To this aim, we propose the following iterative procedure to correct the effects of the spatial averaging on wind LiDAR measurements, which is summarized in the flow chart of Fig. 1.

First, the pre-multiplied spectrum of the radial velocity projected in the horizontal mean wind direction is fitted with the ~~Kaimal~~ spectral model of Eq. 1 only for ~~frequencies~~ wavenumbers smaller than $\cancel{f_{Th}}$ $k_{Th,0} = 2\pi/l$. Indeed, we expect to observe significant spatial-averaging effects for turbulent length scales smaller than the probe length, l. ~~As it will be shown in the following,~~ $\cancel{f_{Th}}$ ~~is determined iteratively and is of the order of~~ $\cancel{\mathcal{O}(10^{-1})}$ ~~Hz~~. For ~~frequencies~~ wavenumbers higher than $\cancel{f_{Th}}$ the selected cutoff value, the ratio between the fitted Kaimal spectrum and the PSD of the LiDAR velocity, φ_*^2, is calculated to quantify the effect of the energy damping due to the LiDAR measuring process. Subsequently, the LiDAR-to-Kaimal ratio, φ_*^2,

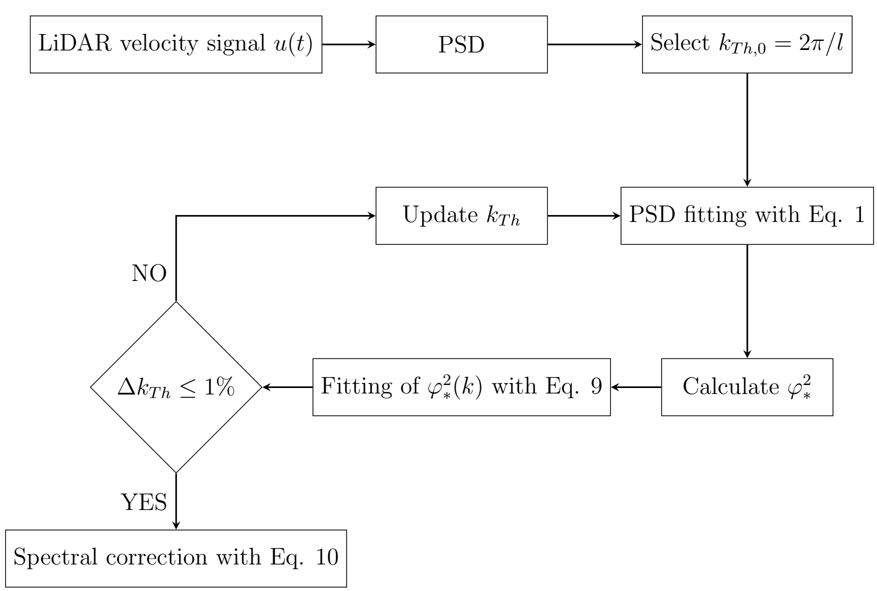

Figure 1. Flowchart for the iterative correction procedure of the LiDAR velocity measurements.

is fitted with Eq. 9 through a least-square algorithm to estimate the filter order, α, and provide an updated value for the cutoff ~~frequency~~ wavenumber, $\cancel{f_{Th}}$ k_{Th}. ~~If the guessed cutoff frequency is larger than the fitted value, the fitting of the LiDAR spectrum with the Kaimal model is repeated updating the value of cutoff frequency. Conversely, if the cutoff frequency calibrated on the LiDAR-to-Kaimal ratio is larger than the guessed value,~~ This process is iterated until convergence on the parameter k_{Th} is achieved (for this work, the convergence condition imposed is a variation of k_{Th} smaller than 1% of the previous value). If during the iterative process, k_{Th} achieves a value equal or smaller than that corresponding to the spectral peak, k_p, then the procedure is arrested and a warning is dispatched indicating that the correction procedure was not successful. This warning condition never occurred for all the data analyzed in this work. Furthermore, it should be considered that when k_{Th} achieves values close to k_p, the part of the velocity spectrum, S_u, used for the fitting procedure with Eq. 1 can be so limited to jeopardize the accuracy of the fitting procedure. Once convergence in k_{Th} is achieved, the corrected velocity spectrum, $\cancel{\tilde{S_L}(f)}$ $\tilde{S_L}(k)$, is calculated as:

$$\cancel{\tilde{S_L}(f) = \frac{S_L(f)}{\tilde{\varphi}^2(f)}}.$$

$$\tilde{S_L}(k) = \frac{S_L(k)}{\tilde{\varphi}^2(k)}. \tag{10}$$

It is noteworthy that in contrast to existing models using pre-defined functions to correct the energy damping of the velocity fluctuations, see e.g. Eqs. 5 and 6 (Sjöholm et al. , 2009; Brugger et al. , 2016; Cheynet et al. , 2017), which require information about the LiDAR probe length and the energy distribution over a pulse, the proposed procedure calculates the characteristics of the damping on the LiDAR velocity signals directly from the experimental data, which leads, as it will be shown in the following, to enhanced accuracy in the correction of the LiDAR velocity spectra. On the other hand, the proposed procedure leverages the surface-layer similarity for the Kaimal spectral model for the streamwise velocity and, thus, it can only be applied for wind LiDAR measurements collected within the ASL.

3 Experimental Setup and selected LiDAR datasets

The present study is based on wind LiDAR measurements collected from three different experimental campaigns. The first dataset was acquired during the period June 9-24, 2018 at the Surface Layer Turbulence and Environmental Science Test (SLTEST), which is part of the U.S. Dugway Proving Ground facility in Utah (GPS location: $40°08'07"N, 113°27'04"W$, UTC offset -6 h). Characterized by an elevation variability of 1 m every 13 km (Kunkel and Marusic , 2006; Metzger and Klewicki , 2001), this facility is located in the South West of the Great Salt Lake and extends for 240 km and 48 km along North-South and East-West directions, respectively. An aerial view of the SLTEST facility is reported in Fig. 2a. During the experiment, the prevailing wind direction was from North-North-East.

The second field campaign was carried out at a test site in Celina, TX (GPS location: $33°17'35.3"$N, $96°49'17.5"$W, UTC offset -5 h), which is a relatively flat terrain with a certain variability in land cover (Fig. 2b). For these two field campaigns,

Figure 2. Aerial views of the test sites: **(a)** SLTEST facility; **(b)** Celina site; **(c)** XPIA campaign at the Boulder Atmospheric Observatory. Source of Google Earth. Black crosses represent the instrument locations. In **(c)**, each LiDAR is labeled with its respective name.

wind velocity measurements were performed with a Streamline XR scanning Doppler pulsed wind LiDAR manufactured by Halo Photonics, whose technical details are reported in Table 1. LiDAR fixed scans were performed with an elevation angle between 1.98° and 10°, while the azimuth angle was set equal to the mean wind direction. The latter was monitored through Vertical Azimuth Display (VAD) scans with an elevation of 25° and a sampling period of about 90 s, or through Doppler Beam Swinging (DBS) scans. DBS or VAD scans were executed hourly to monitor variations in the mean wind direction, while the azimuth angle for the fixed scans was updated automatically at the end of each DBS or VAD scan through the feedback scan mode embedded in the LiDAR software, and using the wind-direction measured at the height of 53 m. ~~For the fixed scans, the sampling frequency was varied between 0.5 and 3.3 Hz, while the probe length was always set equal to 18 m.~~ To investigate possible variations of the averaging process related to the accumulation time, the sampling frequency of the fixed scans was varied between 0.5 Hz and 3.3 Hz, while the range gate was always set equal to 18 m.

The third campaign considered in this study is the eXperimental Planetary boundary layer Instrumentation Assessment (XPIA), performed during the period March 2 - May 31, 2015 at the Boulder Atmospheric Observatory (BAO) research facility in Erie, Colorado. For the XPIA campaign, twelve Campbell CSAT3 3D sonic anemometers were mounted on the BAO meteorological tower at heights of 50 m, 100 m, 150 m, 200 m, 250 m and 300 m above the ground. Each height was monitored with two sonic anemometers pointing towards North-West and South-East, respectively. Three velocity components and temperature were recorded with a sampling rate of 20 Hz. For a complete description of the scanning strategies and the instruments utilized during the XPIA experiment see Lundquist et al. (2017). Fig. 2(c) shows the locations of the ~~used~~ LiDARs used.

In the present study, from the XPIA experiment we focus on tests performed during the period March 21-24, 2015 with a Windcube 200S scanning Doppler pulsed wind LiDAR manufactured by Leosphere. Technical specifications of the Windcube 200S wind LiDAR are reported in Table 1. The LiDAR performed measurements by staring towards one of the sonic anemometers for a period of 14.5 minutes. A sequential scan at four different heights was done for every hour during each day; details

Table 1. Technical specifications of the pulsed scanning Doppler wind LiDARs used for this work, namely a Streamline XR by Halo Photonics and a Windcube 200S by Leosphere.

Parameter	Value	
LiDAR	Streamline XR	Windcube 200S
Wavelength [μm]	1.5	1.54
Repetition rate [kHz]	10	10
Velocity resolution [m s^{-1}]	± 0.0764	< 0.5
Velocity bandwidth [m s^{-1}]	± 38	± 30
Number of FFT points	1024	1024
Measurement range	45 m to 12 km	50 m to 6 km
LiDAR gate length	18 m to 120 m	25 m to 100 m
Number of gates	200	200
Sampling rate	0.5 Hz to 4 Hz	0.1 Hz to 2 Hz

of these tests are available in Debnath (2018). Simultaneous measurements performed with a scanning Doppler wind LiDAR and sonic anemometers are analyzed to assess the proposed spectral correction procedure of LiDAR measurements.

For the Celina and SLTEST field campaigns, the regime of the ~~static~~ atmospheric stability was monitored through sonic anemometers mounted at a height of 3 m in the proximity of the LiDAR location. The sampling frequency of the sonic anemometer data was 20 Hz, while atmospheric stability was characterized through the Obukhov length calculated as follows (Monin and Obukhov , 1954):

$$L = -\frac{\theta_v u_{\tau,S}^3}{\kappa g \overline{w'\theta_v'}}, \tag{11}$$

where $\kappa = 0.41$ is the von Kármán constant, g is the gravitational acceleration, $\overline{w'\theta_v'}$ is the sensible heat flux, θ_v is the average virtual potential temperature (in Kelvin) and $u_{\tau,S}$ is the friction velocity calculated from sonic anemometer data as (Stull , 1988):

$$u_{\tau,S} = \left(\overline{u'w'}^2 + \overline{v'w'}^2\right)^{1/4}. \tag{12}$$

To avoid effects of thermal stratification and buoyancy on our analysis, only datasets acquired under near-neutral conditions are considered, which are selected by imposing the threshold: $|z/L| \le 0.05$ (Kunkel and Marusic , 2006; Liu et al. , 2017).

The LiDAR velocity signals undergo a quality control process to ensure statistical significance and accuracy of the measurements. ~~For the SLTEST and Celina campaigns, LiDAR fixed scans were performed with the laser beam aligned in the mean wind direction, which is monitored hourly through DBS or VAD scans~~. Only datasets with a variability of the 10-minute averaged wind direction within the range $\pm 20°$ have been considered to avoid significant offset between the LiDAR azimuth angle and the instantaneous wind direction (Hutchins et al. , 2012).

The quality of the LiDAR signals is then checked based on the intensity of the back-scattered signal. For the Windcube 200S LiDAR, the samples with a carrier-to-noise ratio (CNR) higher than -25 dB are selected, while for the Streamline XR LiDAR data are analyzed only if the intensity of the back-scattered signal is higher than 1.01.

The statistical steadiness of the LiDAR signals is estimated through the non-stationary index (IST) calculated as follows (Liu et al. , 2017):

$$IST = \frac{CV_m - CV_{tot}}{CV_{tot}}, \tag{13}$$

where:

$$CV_m = \frac{1}{N}\sum_{j=1}^{N} CV_j. \tag{14}$$

In Eq. 14, CV_j is the variance of a signal subset with a duration of 5 minutes, while N is the total number of subset signals generated without overlapping; CV_{tot} is the variance of the signal over the entire period. For Celina and SLTEST campaigns, IST was calculated for 1-hour periods, while for the XPIA deployment the whole 14.5-minute record was analyzed. For quality control purpose, signals with $IST \geq 40\%$ are usually rejected (Foken et al. , 2004; Liu et al. , 2017). The IST is calculated for each range gate and the maximum IST value for the selected datasets is reported in the eighth column of Table 2.

Subsequently, a gradient-based procedure is used to remove outliers from the LiDAR radial velocity signals. Specifically, the partial derivative in time of the radial velocity is calculated through a second-order central finite-difference scheme, and velocity samples with absolute partial derivative larger than 15 times the respective median value calculated over the entire signal are marked as outliers and replaced through the inpaint-nans function available in Matlab (D'Errico , 2004). The used threshold value is selected based on a sensitivity analysis. ~~which are replaced through a least-squares approach in time for each LiDAR gate under investigation. Each signal is linearly detrended in time over the whole duration in order to remove large-scale fluctuation, while keeping turbulent velocity fluctuations.~~ Based on the above-mentioned quality-control procedure, five datasets were selected, whose details are reported in Table 2.

Table 2. Description of the selected datasets: Φ is the LiDAR elevation angle, f_S is the sampling frequency, l is the probe length, IST is the maximum value of the non-stationary index, u_τ is the friction velocity, and z_0 is the aerodynamic roughness length. The last column reports the symbol used for each dataset.

Date	Dataset	LiDAR	UTC Time	Φ [°]	f_s[Hz]	l[m]	max. IST [%]	u_τ [m s^{-1}]	z_0 [mm]	Symbol
23 March 2015	XPIA	Windcube	14:15 - 14:29	5.00	2	50	19.1	0.179	-	-
10 June 2018	SLTEST		10:00 - 13:00	3.50	1	18	24.6	0.414	$2.1 \cdot 10^{-2}$	×
26 May 2017	Celina1		23:35 - 00:35	10.00	3.3	18	24.1	0.479	15	●
02 October 2017	Celina2	Streamline	22:10 - 01:10	5.00	0.5	18	37.7	0.526	87	■
26 January 2018	Celina3		20:30 - 23:30	1.98	1	18	39.7	0.404	17	▼

The radial velocity, V_r, measured by a Doppler wind LiDAR, as explained in §2, is expressed as:

$$V_r = V_h \cos(\theta - \theta_w)\cos\Phi + W \sin\Phi \tag{15}$$

where θ and Φ are the LiDAR azimuth and elevation angles, respectively, θ_w is the wind direction, V_h and W are the horizontal and vertical wind velocities, respectively. As previously mentioned, for the SLTEST and Celina field campaigns, LiDAR measurements were carried out with the azimuth angle equal to the mean wind direction and very low elevation angles (Table 2). Therefore, we can calculate an approximation of the horizontal wind speed as:

$$U_{eq} = V_r / \cos\Phi, \tag{16}$$

which is referred to as horizontal equivalent velocity. In the following, U_{eq} is considered to calculate the streamwise velocity spectrum. Furthermore, the variance of the radial velocity is the first-order approximation of the streamwise-velocity variance given the above-mentioned setup constraints (Eberhard et al. , 1989; Sathe and Mann , 2013).

4 Assessment of the LiDAR spectral correction against sonic anemometry

In this section, the procedure proposed in §2 to correct the energy damping in the LiDAR velocity measurements due to the energy pulse distribution over the ~~range gate~~ probe volume is assessed against sonic anemometry by leveraging the XPIA dataset, whose characteristics are summarized in Table 2. LiDAR fixed scans were performed with an elevation angle of $5°$ to have one range gate in the proximity of a sonic anemometer installed on the BAO tower at a height of 100 m. The LiDAR ~~range gate~~ probe length used for that experiment was equal to 50 m, while the sampling rate was set equal to 2 Hz.

Based on the instantaneous wind direction measured by the sonic anemometer and neglecting the vertical velocity due to the very low elevation angle of the LiDAR laser beam, the horizontal equivalent velocity, U_{eq}, is calculated from the LiDAR radial velocity through Eq. 15 and it is reported in Fig. 3 with a blue line. The ~~PSD of the~~ LiDAR equivalent velocity, U_{eq}, is then high-pass filtered to remove low-frequency non-turbulent velocity fluctuations, using the following spectral transfer function:

$$G(k;\beta,k_{co}) = \frac{1 + \tanh\left[\beta \cdot \log\left(\frac{k}{k_{co}}\right)\right]}{2}, \tag{17}$$

where k_{co} is the cutoff wavenumber, which should be smaller than k_p to avoid effects on the spectral peak. The parameter β is set equal to 100 to generate a sufficiently sharp filter across the cutoff wavenumber, k_{co} (Hu et al., 2019). The PSD of the velocity signal high-pass filtered with a cutoff wavenumber $k_{co} = 1.26 \times 10^{-3}$ m^{-1} is reported in Fig. 4(a) with a grey line.

In case significant noise in the velocity spectra is observed in the proximity of the Nyquist wavenumber, see e.g. Debnath (2018), as for this velocity signal, a denoising procedure is then applied to remove possible noise effects on the velocity signals. Following the wavelet-transform-based procedure proposed by To et al. (2009), the velocity signal is decomposed in a 10-level orthogonal wavelet basis. For each level, a soft-threshold selection is applied to the wavelet coefficients to remove those related

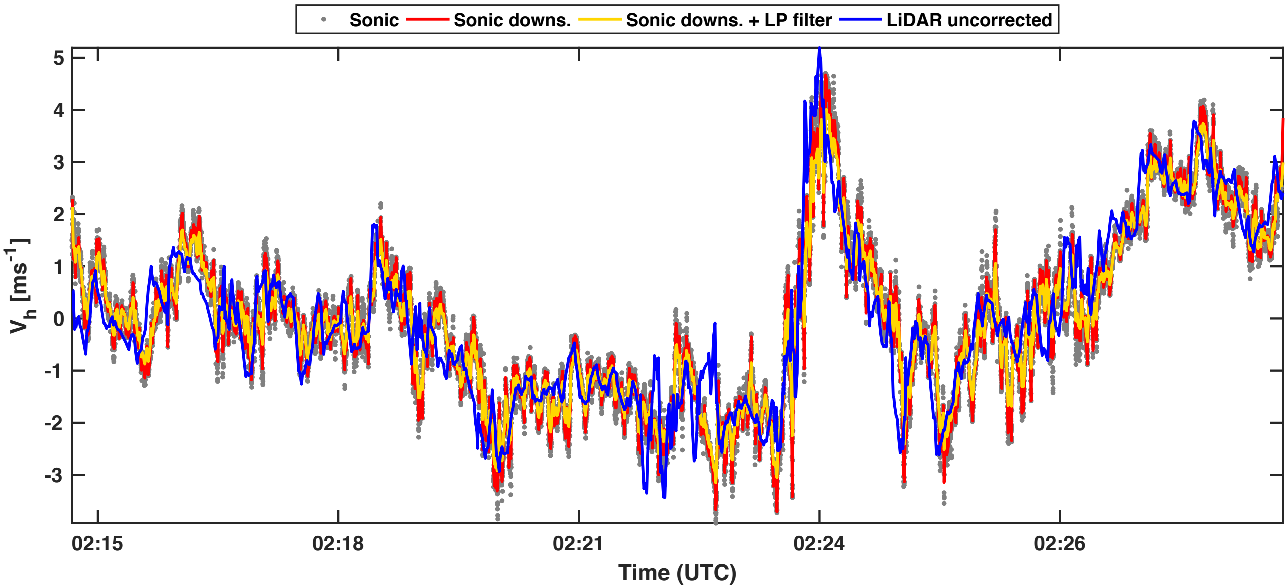

Figure 3. Subset of the horizontal velocity measured with a LiDAR and sonic anemometer from the XPIA dataset. The grey dots represent the original 20-Hz-sampled sonic-anemometer data; the red line is the sonic anemometer signal downsampled at 2 Hz; the yellow line is the sonic anemometer signal after the convolution of Eq. 9; the blue line is the LiDAR signal before the spectral correction.

to noise. The estimated noise-free wavelet coefficients, d_{jk}, are calculated as:

$$d_{jk} = \begin{cases} \mathrm{sgn}(w_{jk})(|w_{jk}| - T_j) & \text{if } |w_{jk}| > T_j \\ 0 & \text{otherwise} \end{cases}, \tag{18}$$

where $j = 1, ..., 10$ is the number of levels in the wavelet basis; $k = 1, ..., 2^j$ and w_{jk} are the coefficients of the discrete wavelet transform of the original signal. T_j represents a noise-based threshold for the j^{th} level, that for this work is set to (To et al. , 2009):

$$T_j = \frac{\mathrm{med}(|w_{jk}|)}{0.67} \cdot \sqrt{2 \log 2^j}, \tag{19}$$

where $\mathrm{med}(\cdot)$ stands for the median value. Finally, the denoised signal is reconstructed in time through the modified wavelet coefficients d_{jk}. The spectrum of the denoised LiDAR velocity signal is reported in Fig. 4(a) with a light-blue line.

For modeling purpose, the velocity spectra are then smoothed in the wavenumber domain following the Savitztky-Golay filter (Savitzky and Golay , 1964), by using a second-order polynomial function and windows with the width equal to $\mathrm{int}[10(160k)^{0.5}]$, where k is in m^{-1} and int is rounding to the closest integer number (Balasubramaniam , 2005). ~~Specifically, the energy spectrum is smoothed with a moving average over intervals whose length increases with the frequency, followed by a best-fit with a second-order polynomial function.~~ The result is an increased level of smoothness moving towards the Nyquist ~~frequency~~ wavenumber. The LiDAR velocity spectrum resulting from the de-noising and smoothing procedures is reported in Fig. 4(a) with a blue line. The PSD of the LiDAR velocity is then fitted through the spectral model (Eq. 1) producing the following fitting parameters: ~~$A_f = 336.1$ s, $B_f = 355.3$ s,~~ $A = 23.3$, $B = 24.7$. The resulting Kaimal spectrum is plotted in Fig. 4(a) with a black line.

A deviation of the LiDAR velocity spectrum from the $-5/3$ scaling of the inertial sub-range is observed ~~for $kl/(2\pi) \gtrapprox 0.4$,~~ due to the LiDAR measuring process over the ~~range gate~~ probe volume. The ratio between the fitted Kaimal spectrum and the LiDAR velocity spectrum, $|\varphi_*|^2$ in Fig. 4(b), is then fitted with Eq. 9 to estimate the low-pass filter of order α and cutoff ~~frequency~~ wavenumber, $\cancel{f_{Th}}$ k_{Th} . For this LiDAR velocity signal, α is equal to 0.774 and $k_{th}l/(2\pi) \approx 0.8$, with an R^2 value of 0.702, which confirms the proposed model is a good approximation for the damping of the velocity fluctuations over the LiDAR ~~range gate~~ probe volume. In Fig. 4(b), the weighting functions of Eqs. 5 and 6 are also reported for a ~~range gate~~ probe length $l =$50 m.

To assess the accuracy of the estimated low-pass filter in representing the LiDAR averaging process over a ~~range gate~~ probe volume, first we apply the estimated low-pass filter to the simultaneous and co-located sonic anemometer velocity signal. The horizontal velocity retrieved from the sonic anemometer is first down-sampled with the sampling frequency of the LiDAR measurements, namely 2 Hz, using the Matlab function "decimate" with a finite-impulse response (FIR) low-pass filter with order equal to 10 (Weinstein , 1979). The resulting down-sampled velocity signal is reported with a red line in

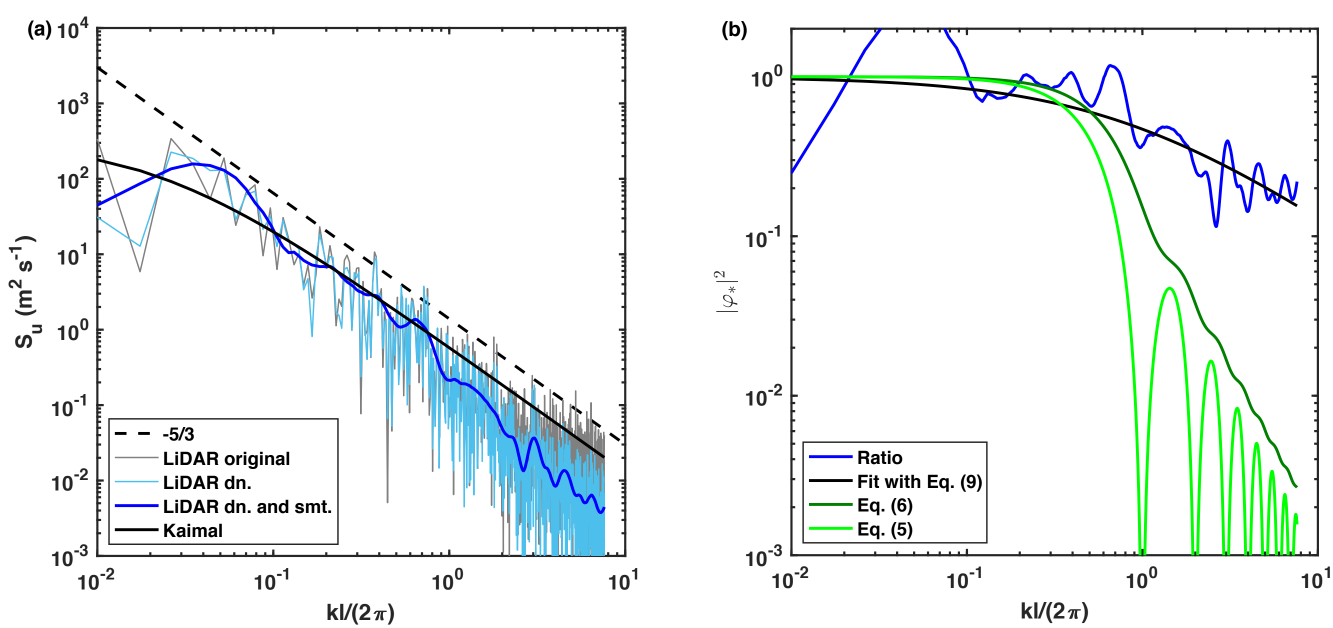

Figure 4. Correction of the LiDAR velocity spectrum from the XPIA dataset: **(a)** velocity spectra of the raw LiDAR data (grey), LiDAR data after application of the de-noising procedure (To et al. , 2009) (light blue), LiDAR data after smoothing procedure (dark blue), Kaimal spectrum (black) and $-5/3$ slope (black dashed); **(b)** $|\varphi_*|^2$ (blue), $|\varphi_*|^2$ fitted with Eq. 9 (black); predictions from Eq. 5 (dark green) and Eq. 6 (bright green) are reported as well.

Fig. 3, and the respective PSD in Fig. 5(a). Subsequently, the down-sampled sonic-anemometer signal is low-pass filtered with the filter of Eq. 9 modeled only using the LiDAR data (yellow line in Fig. 3 and in Fig. 5(a)). The comparison in Fig. 3 of the sonic anemometer signal down-sampled and low-pass filtered with the LiDAR raw signal already highlights a very good agreement, which suggests that the energy damping carried out by the LiDAR pulse over the ~~range gate~~ probe volume is well represented through the proposed low-pass filter. This feature is further corroborated by the respective spectra reported in Fig. 5(a). Specifically, the ~~spectrum of the LiDAR signal~~ spectrum of the LOS velocity has the same slope in the inertial sub-range of the sonic-anemometer signal down-sampled and low-pass filtered, while some differences are observed for lower frequencies, which are most probably due to the different size of the measurement volume of the two instruments, namely 50 m for the LiDAR and 0.3 m for the sonic anemometer.

The comparison between LiDAR and sonic anemometer data is now presented through a linear regression analysis, which is reported in Fig. 6. The LiDAR horizontal equivalent velocity, U_{eq}, is analyzed against the horizontal wind speed measured by the sonic anemometer before (Fig. 6(a)) and after (Fig. 6(b)) the low-pass filtering. All the linear regression parameters improve for the low-pass filtered sonic anemometer data: the slope increases from 0.878 to 0.962, the R-square value increases from 0.88 to 0.904, and the correlation coefficient, ρ, increases from 0.88 to 0.904.

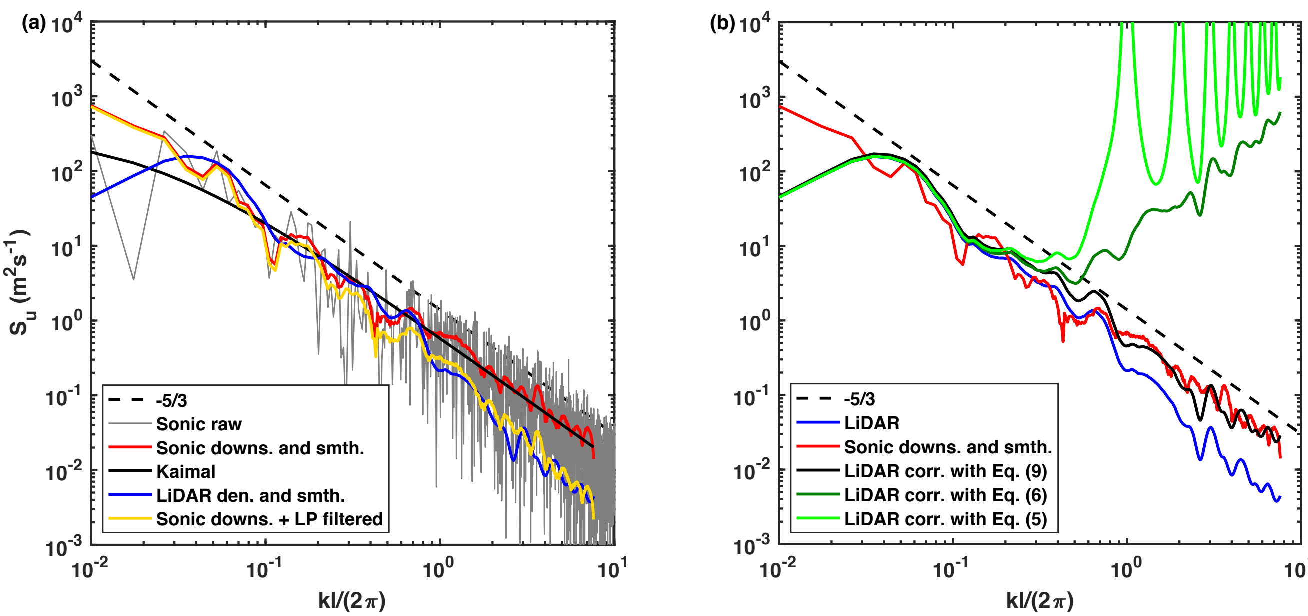

Figure 5. Comparison of LiDAR velocity data against sonic anemometry data for the XPIA dataset: **(a)** raw sonic anemometer data (grey), down-sampled and smoothed sonic-anemometer (red), Kaimal model (black) tuned on the LiDAR velocity spectrum (blue), sonic anemometer signal down-sampled and low-pass filtered (yellow); **(b)** LiDAR velocity spectrum (blue), down-sampled and smoothed sonic anemometer spectrum (red), LiDAR spectrum corrected with Eq. 9, 5 and 6 (black, dark and bright green lines, respectively).

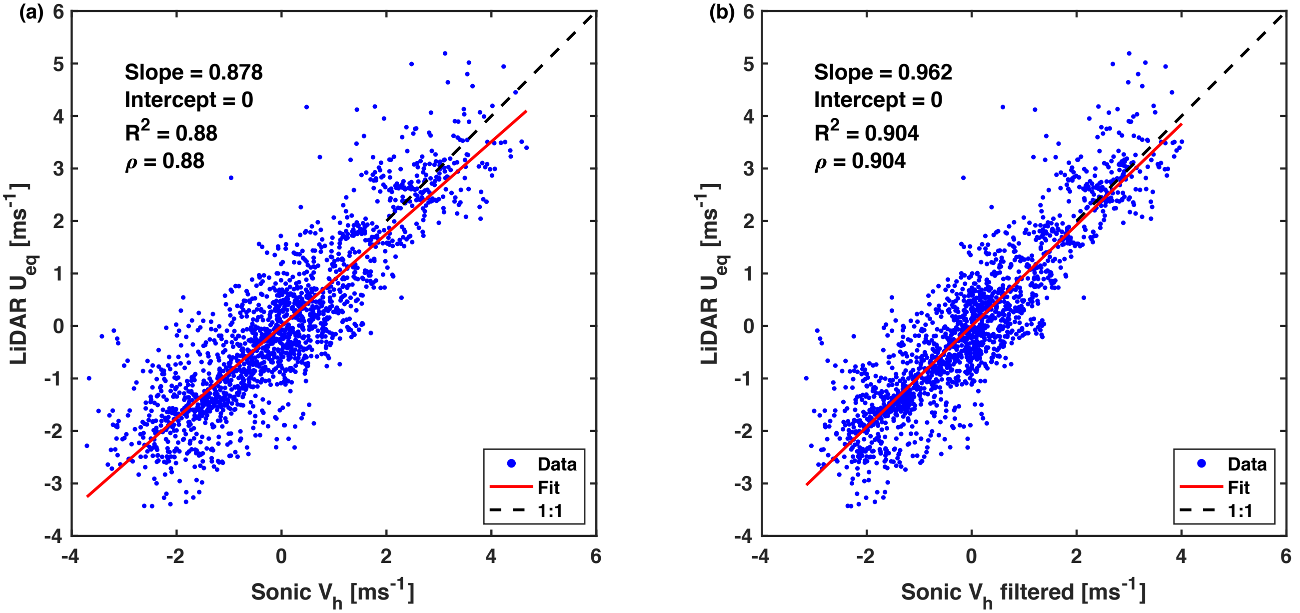

Figure 6. Linear regression between LiDAR horizontal equivalent velocity, U_{eq}, and sonic anemometer horizontal velocity from the XPIA dataset: **(a)** raw data from the sonic anemometer; **(b)** sonic anemometer data down-sampled and low-pass filtered.

We now aim to correct the LiDAR velocity signal from the energy damping due to the laser pulse distribution over the ~~range gate~~ probe volume. First, the LiDAR velocity spectrum is corrected by using the existing models of Eqs. 5 and 6 with $l = 50$ m, i.e. the used LiDAR ~~range gate~~ probe length. As shown in Figs. 4(b) and 5(b), these correction methods largely over-estimate the turbulent energy for ~~frequencies~~ wavenumbers larger than ~~f_{Th}~~ k_{Th} or, in other words, the characteristic length scale should be smaller than the LiDAR ~~range gate~~ probe length to provide reasonable spectral corrections. A possible explanation for the poor performance of these deconvolution models could be the different probe ~~gate~~ length used for the XPIA campaign ($l = 50$ m) in contrast to $l = 30$ m used in the original study of this deconvolution model (Mann et al. , 2009) , and the presence of measurement noise in the data, which is not accounted for in the models of Eqs. 5 and 6.

According to the correction technique proposed in this paper, the LiDAR velocity spectrum can now be corrected for the averaging process by reversing the effect of the estimated low-pass filter through Eq. 10. The corrected velocity spectrum is reported in Fig. 5(b) with a black line. The velocity spectrum of the corrected LiDAR velocity signal clearly shows that the expected slope of $-5/3$ in the inertial sub-range is recovered, while the spectral energy for ~~frequencies~~ lower wavenumbers ~~lower than f_{Th}~~ are practically unchanged.

~~To provide more insight on the temporal consistency between the corrected LiDAR time-series and the sonic anemometer data, we band-pass filter LiDAR and sonic anemometer data between the selected cutoff frequency $f_{th} = 0.04$ Hz ($kl/(2\pi) \approx 0.4$) and the Nyquist frequency of the LiDAR measurements, i.e. 1 Hz. Indeed, this is the frequency range more affected by the smoothing process over the probe volume and, thus, requiring more correction of the spectral energy. The filtered velocity sig-~~

~~nals are subdivided into sub-periods with duration $1/f_{th} = 25$ s, and the standard deviation of the wind velocity is calculated. The linear regression analysis of the velocity standard deviation calculated from the sonic anemometer data and the LiDAR data before and after the spectral correction (reported in Figs. 7(a) and (b), respectively) highlights the positive effect of the spectral correction on the second-order statistics of the LiDAR measurements. For the linear regression of the velocity standard deviation, after the spectral correction the slope increases from 0.674 to 1.083 and the intercept reduces from 0.132 to -0.022, while the remaining parameters are essentially unaltered.~~

5 Variability of the low-pass filter parameters

For the SLTEST and Celina field campaigns, LiDAR velocity measurements were collected for time periods between 2 and 3 hours (see Table 2). The procedure used to obtain the streamwise velocity spectra is the following: for each LiDAR velocity signal, the high-pass filter of Eq. 17 is applied with a cutoff wavenumber $k_{co} = 0.001$ m^{-1} to remove low-frequency velocity fluctuations connected with atmospheric mesoscales. The PSD of each velocity signal is then calculated with the pwelch function implemented in Matlab (Welch , 1967) without window overlapping and window width corresponding to k_{co}. Subsequently, smoothing of the velocity spectra is carried out through the Savitzky-Golay filter, as detailed in the previous section (Savitzky and Golay , 1964; Balasubramaniam , 2005).

The ~~first- and second-order statistics~~ mean values and variance of the LiDAR equivalent velocity are plotted in Figs. 7(a) and (b), respectively. For the mean velocity field in Fig. 7(a), while a logarithmic region is generally observed at the lower heights, a noticeable difference in terms of terrain roughness between the SLTEST and Celina sites reflects in different vertical intercepts and respective aerodynamic roughness length. The latter is estimated to be equal to 0.021 mm for SLTEST and, as average, 37 mm for the Celina site.

~~The different surface roughness of the two sites also affects the variance of the equivalent horizontal velocity, which is~~ The vertical profiles of streamwise velocity variance are reported in Fig. 7(b) as a function of height. For the datasets collected at the Celina site, a general increase of the velocity variance is observed with increasing height. Specifically, for the dataset Celina1, after achieving a maximum value at height $z \geq 40$ m, a quasi-logarithmic reduction of the velocity variance is observed with increasing height, which is in agreement with previous laboratory and numerical studies of canonical boundary layer flows (Kunkel and Marusic , 2006; Meneveau and Marusic , 2013). A logarithmic reduction of the velocity variance with increasing height is also observed for the SLTEST dataset throughout the entire height-range.

For the SLTEST dataset, the PSD of the LiDAR velocity signals acquired at the different gates from 10 m up to 60 m with a vertical spacing of 1 m are plotted in Fig. 8. A departure from the expected $-5/3$ slope in the inertial sub-range is observed ~~starting from $f \gtrapprox 0.1$ Hz~~ for wavenumbers larger than 0.07 m^{-1}. ~~Considering the observed spectral energy damping, the Kaimal model for the streamwise turbulence (Eq. 1) is fitted on the measured LiDAR velocity spectra only for frequencies with $f \lessapprox 0.1$Hz~~. The ~~fitted~~ Kaimal spectra, which are obtained by fitting the measured LiDAR velocity spectra only for wavenumbers lower than the respective k_{Th} for each height, are reported in Fig. 9(a) for the lowest and highest range gates. The ratio between the LiDAR and Kaimal spectra, $|\varphi_*|^2$, is then calculated and fitted through Eq. 9 to estimate the order and cutoff

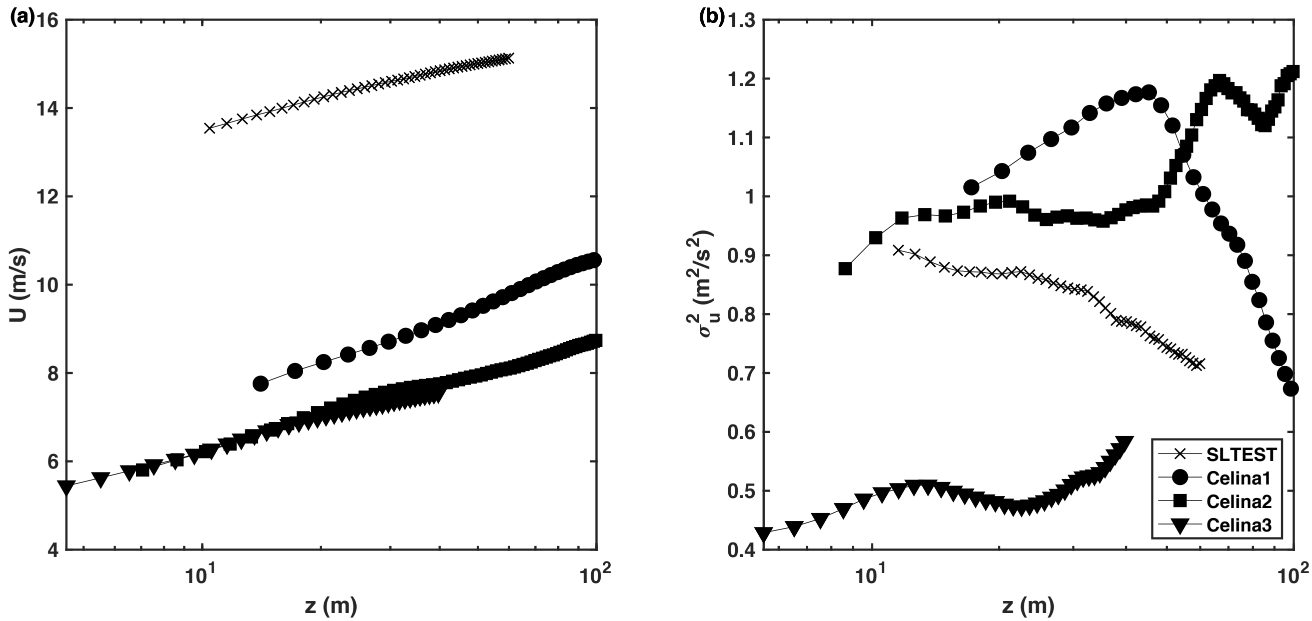

Figure 7. First- and second-order statistics of the equivalent velocity, U_{eq}, as a function of height for the various datasets: **(a)**: mean value; **(b)**: variance.

~~frequency~~ wavenumber of the respective low-pass filter (Fig. 9(b)). For the lowest gate at height of 10 m, the fitting procedure estimated $\alpha = 5.08$ and ~~$f_{Th} = 0.14$ Hz~~ $k_{Th} = 0.065\ \mathrm{m}^{-1}$, while for the highest range gate at height of 60 m $\alpha = 4.16$ and ~~$f_{Th} = 0.16$ Hz~~ $k_{Th} = 0.066\ \mathrm{m}^{-1}$.

~~Results of the correction procedure applied to the SLTEST dataset are shown in Fig. 11. It is noteworthy to observe that the fitting of the LiDAR spectra allows detecting the typical decrease in frequency of the energy peak with increasing height (reported with black triangles in Fig. 11(b)), which is connected with the increase of the integral length scale The correction of the LiDAR spectra keeps unaltered the energy content of the large energy-containing turbulent structures, while a significant correction is performed within the inertial sub-range to improve accuracy in the estimate of the turbulent statistics.~~

Since the correction procedure is based on two consecutive best-fit operations, the robustness of the model is assessed for each LiDAR gate through the R-square value of the respective fitting procedure. ~~Regarding the fitting of the LiDAR spectra with the Kaimal model of Eq. 1, the R-square value is plotted in Fig. 11(a) for all the heights and available datasets.~~ All the datasets generally show a very good agreement between experimental data and the ~~Kaimal~~ spectral model, i.e. $0.82 \leq R^2 \leq 0.98$, with the SLTEST dataset showing the highest level of agreement ($R^2 \geq 0.96$). ~~To quantify~~ Accuracy in modeling the actual energy damping due to the LiDAR measuring process through the low-pass filter of Eq. 9 is quantified through the R-square value of the fitting procedure of the experimental energy damping, φ_*^2, with the analytical model of Eq. 9. The R-square values result to be always larger than 88%, corroborating the good approximation for the proposed model. ~~of each fitted function is plotted in Fig. 11(b).~~

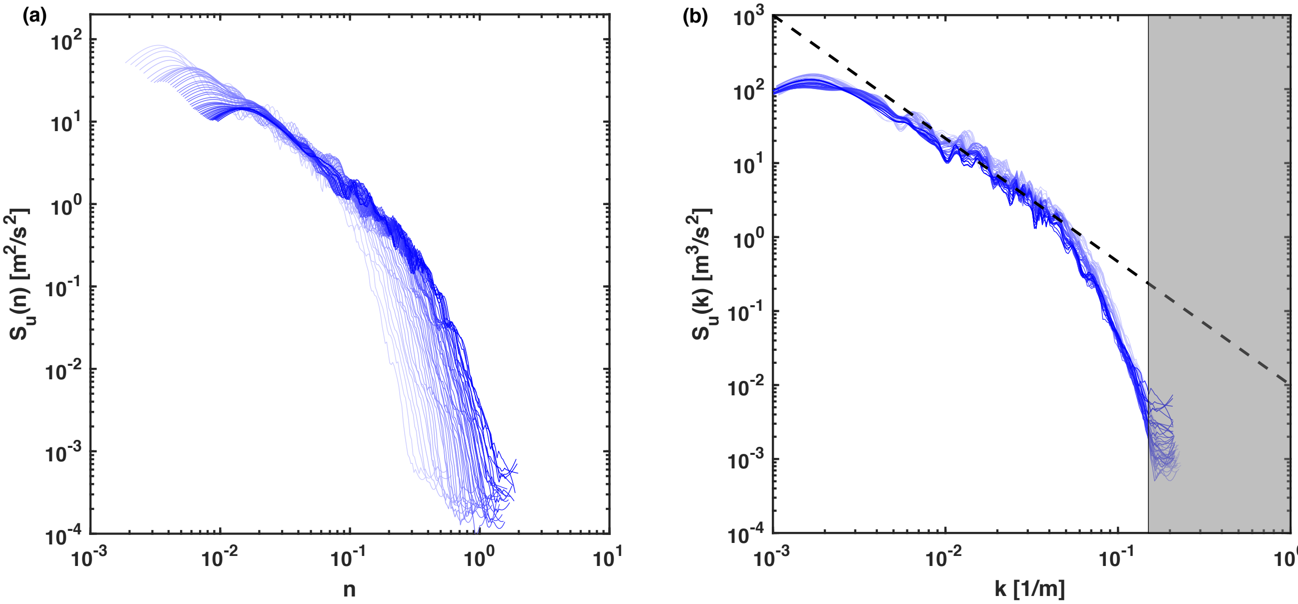

Figure 8. Velocity spectra for the SLTEST dataset at different heights: **(a)** spectra as a function of the reduced frequency, n; **(b)** spectra as a function of the wavenumber, k. Line color is darker with increasing height. The black dashed line represents the $-5/3$ slope. In (b), the shaded area covers the noisy part of the velocity spectra.

The proposed spectral correction of the LiDAR measurements is now applied to all the ~~selected~~ datasets collected at the Celina and SLTEST sites (see Table 2). As explained in §2, the first step of the proposed procedure consists in fitting each velocity spectrum with the ~~Kaimal~~ spectral model of Eq. 1. In the right column of Fig. 10, the results of this operation are reported for all the datasets of the SLTEST and Celina field campaigns. The ~~Kaimal~~ spectral model (depicted with a red line) has been fitted on the uncorrected LiDAR spectrum (blue lines) using a cutoff wavenumber, k_{Th}, estimated for each velocity signal using the iterative procedure illustrated in Fig. 1. In the figures, line colors become darker with increasing height. For the sake of clarity, the fitted Kaimal spectrum is only shown for the highest LiDAR range gate.

The second step of the correction procedure consists of approximating the LiDAR-to-Kaimal spectral ratio with the low-pass filter of Eq. 9. Firstly, the energy ratio is quantified for each LiDAR range gate, as reported in the left column of Fig. 10. We can observe that the ratio always settles about the unit at the lowest range of the spectral domain, while it monotonically reduces from the cutoff ~~frequency~~ wavenumber towards the Nyquist ~~frequency~~ wavenumber, which is an effect of the LiDAR measuring process. By plotting $|\varphi_*|^2$ as a function of $\cancel{(f/f_{Th})^\alpha}$ $(k/k_{Th})^\alpha$, ~~a quasi self-similar behavior is observed among the various range gates, which represents a further assessment of the accuracy of the proposed correction procedure.~~ all the estimated transfer functions practically collapse on the same curve for measurements collected at different heights. The latter is then compared with the analogous of Eqs. 5 and 6.

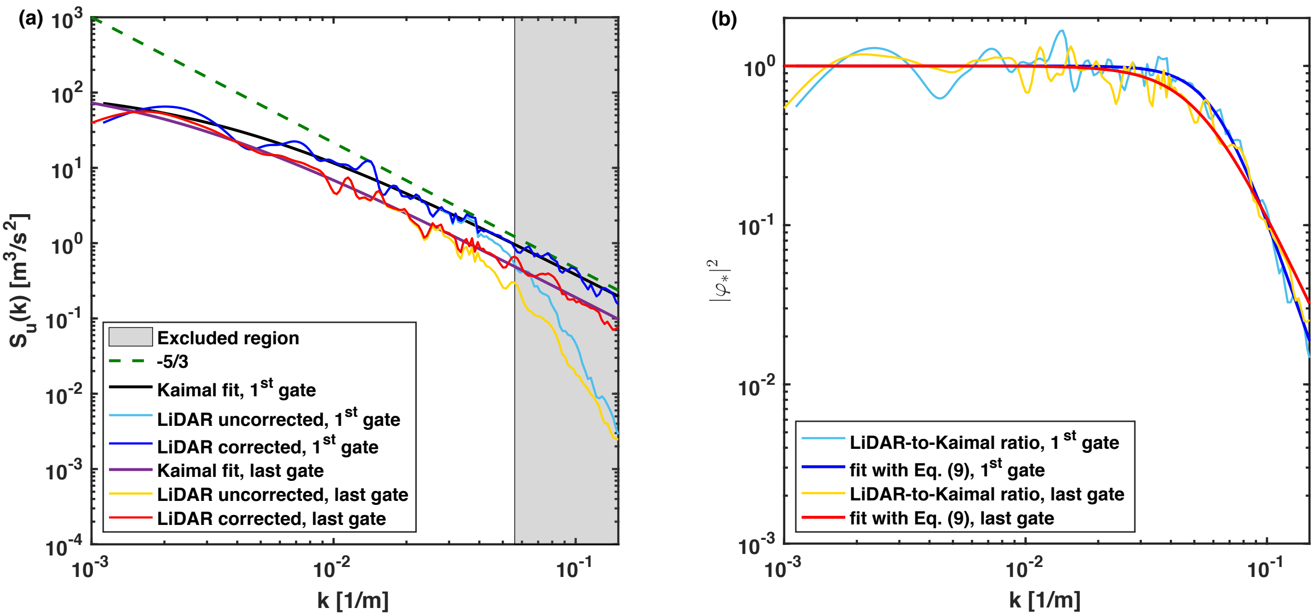

Figure 9. LiDAR velocity signals from the SLTEST dataset acquired at $z = 10$ m (first gate, dark and light blue lines) and $z = 60$ m (last gate, red and yellow lines): **(a)** correction of the LiDAR spectra; **(b)** ratio between LiDAR and Kaimal spectra, φ_*^2, and low-pass filter fitted with Eq. (9).

As the last step, to retrieve the corrected LiDAR velocity spectra, the original spectrum is divided by the modeled correction function, $|\tilde{\varphi}|^2$ (Eq. 10). These corrected LiDAR velocity spectra are reported on the right column of Fig. 10, where we can observe that the $-5/3$ slope of the inertial sub-range is always recovered. The LiDAR spectra corrected with the models of Eq. 5 and 6 are also reported to highlight the improved accuracy achieved through the proposed method. In particular, it is observed that the existing models of Eqs. 5 and 6 always under-estimate the spectral energy attenuation; thus, for the actual choices of gate length and sampling rates, a data-driven approach is preferred to correct the LiDAR smoothing effect.

The corrected variance of the LiDAR velocity signals is compared with the respective quantity calculated for the raw LiDAR data in Fig. 11(a). As expected, the wall-normal profile of the variance calculated as integral of the de-convoluted spectrum is considerably larger than the respective value obtained from the convoluted spectrum, indicating that the underestimation related to the spatial averaging is significant. To quantify the effects of the spectral correction on the LiDAR data, the relative percentage increment of variance is calculated from the smallest frequency up to the noise-free high-frequency content as in Cheynet et al. (2017):

$$\epsilon_{\%} = \frac{\sigma_C^2 - \sigma_U^2}{\sigma_C^2} \cdot 100, \tag{20}$$

where σ_C^2 and σ_U^2 are the corrected and uncorrected, respectively, streamwise velocity variance. The parameter $\epsilon_{\%}$ is reported as a function of height in Fig. 11(b). The underestimation in the velocity variance through the LiDAR measurements seems to

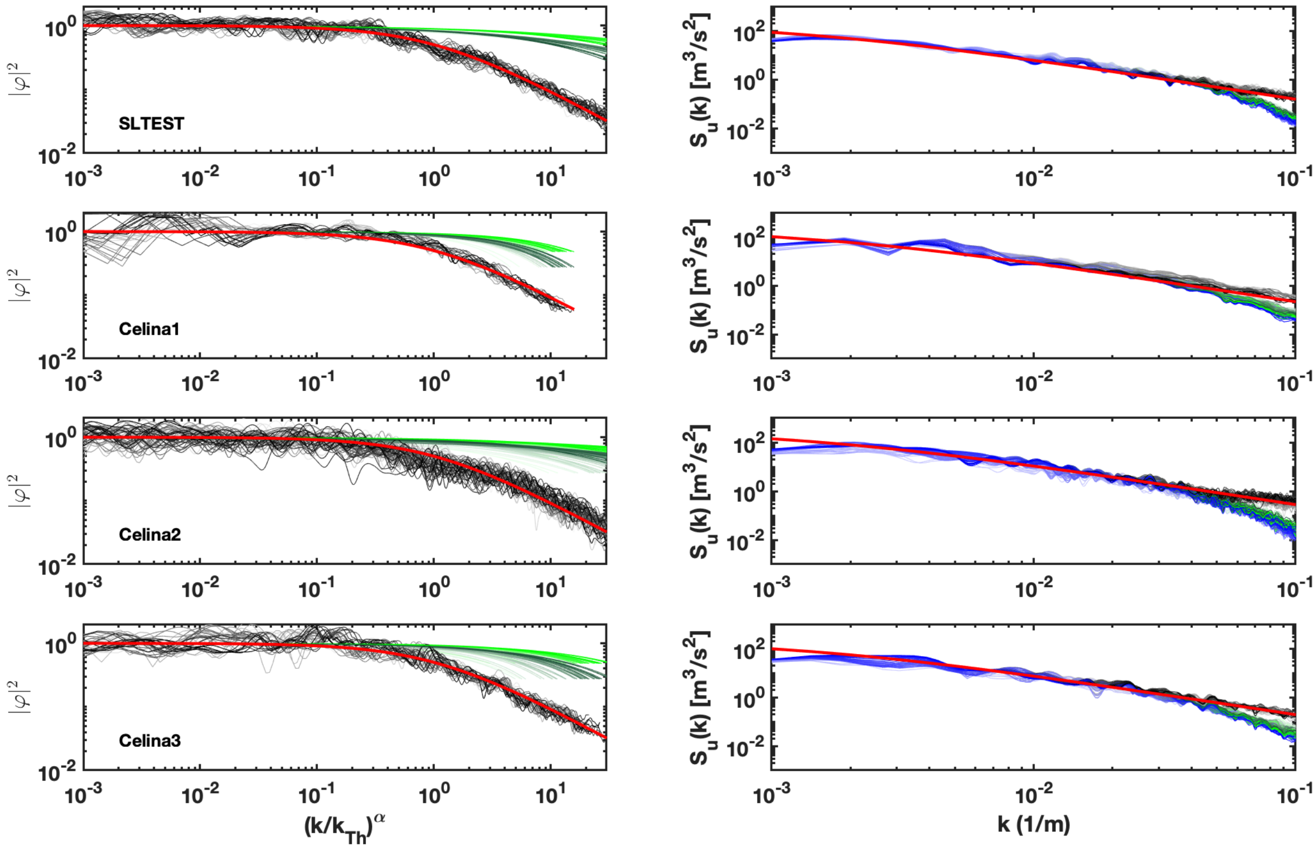

Figure 10. Correction of the LiDAR spectra. Left column: black lines are φ_*^2, the red line is the fitted low-pass filters of Eq. (9) for the highest range gate. Dark and light green lines represent the ~~convolution~~ transfer function predicted by Eqs. (5) and (6). Right column: blue lines are raw LiDAR spectra, dark and light green lines are LiDAR spectra corrected with Eqs. (5) and (6), respectively, the red line is the fitted Kaimal spectrum for the highest range gate and black lines are the LiDAR spectra corrected with the proposed procedure of Fig. 1. Line colors become darker with increasing height.

change with the wall-normal location for the SLTEST dataset and the highest portion of Celina1 ($z > 30$m); for the remaining datasets, the percentage error does not change with height. To clarify this aspect, in the next section we will ~~leverage synthetic turbulent velocity signals to better understand the variability of the LiDAR averaging effect in relation with the size of turbulent structures crossing the probe~~ investigate the variability of the effects of the LiDAR spatial averaging for different mean wind speed, standard deviation and sampling height.

For the SLTEST dataset (see Table 2), the correction of the velocity variance obtained with the proposed method (red marker in Fig. 12a) is compared with those obtained from Eq. 5 (dark green symbols), Eq. 6 (light green marker) and the method of Brugger et al. (2016) (blue marker). For the latter, a probe length of 18 m and a Full-Width Half-Maximum (FWHM) of the

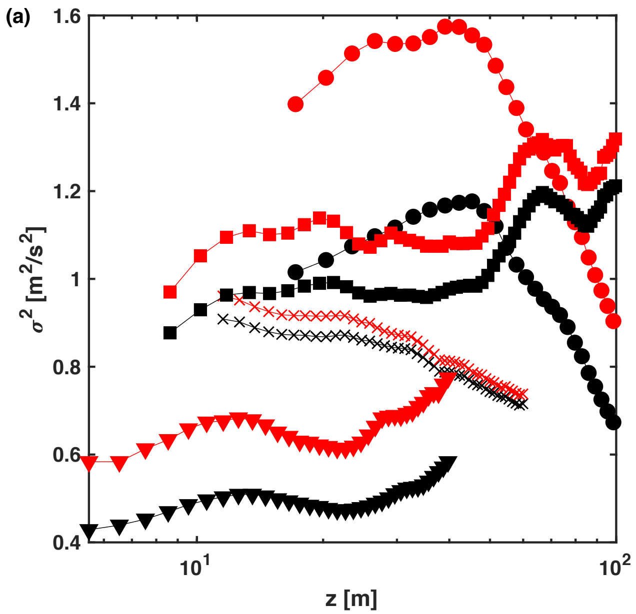

Figure 11. Correction of the second-order statistics: **(a)** Variance before (black) and after (red) the LiDAR spectral correction; **(b)** percentage increment of the velocity variance ($\epsilon_{\%}$) achieved with the LiDAR spectral correction.

laser pulse for the Streamline XR Doppler LiDAR equal to 35 m are used (Risan et al. , 2018). Consistently with the spectra of Fig. 10, the correction methods of Eqs. 6 and 5 under-estimate the effects of spatial averaging of the streamwise velocity variance and they do not allow the complete recovery of the -5/3 slope of the inertial sub-range. The correction based on the structure function proposed by Brugger et al. (2016) leads to a variance distribution larger than what is estimated by the new method based on the Kaimal spectral model, yet with percentage correction in the same order of magnitude (Fig. 12b).

We now focus on the variability of the parameters of the low-pass filter of Eq. 9 among the various datasets. Median and interquartile (IQ) range calculated over the height for the various datasets are reported in Table 3 for both order, α, and cutoff wavenumber, k_{Th}, of the low-pass filter of Eq. 9. First, the order of the low-pass filter, α~~, which is reported in Fig.15(a)~~, is found to be roughly constant over the height for the datasets Celina1 and Celina3, while it decreases with height for the SLTEST and Celina2 datasets. Among the various datasets analyzed, the filter order α has values from 2.2 up to 4.9, a variation entailing limited effects in the correction of the spatial averaging on the LiDAR measurements (not shown here for the sake of brevity). The mean IQ range of α among the various datasets is 0.399. The cutoff ~~frequency~~ wavenumber of the low-pass filter, ~~f_{Th}~~ k_{Th}, is practically constant with height (mean IQ range of 0.022) and has a mean value among the various datasets of: $k_{Th} l/(2\pi)$ =0.163. ~~as shown in Fig. 15(b). In Fig. 15(c), the equivalent cutoff wavelength, λ_{Th} (obtained via Taylor frozen hypothesis) is reported as ratio of the gate length.~~

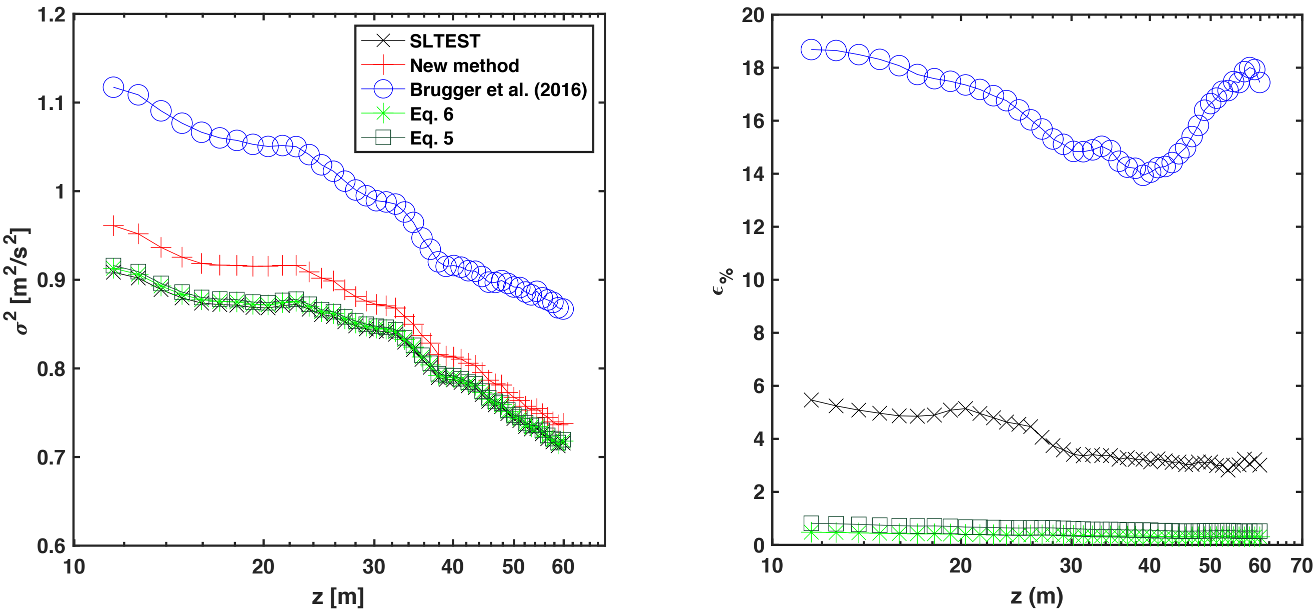

Figure 12. Correction of the streamwise velocity variance with different methods for the SLTEST dataset: **(a)** streamwise velocity variance; **(b)** percentage correction of the velocity variance, $\epsilon_{\%}$. The marker colors are black for the raw LiDAR data, red for the proposed method, light green for Eq. 6, dark green for Eq. 5, and blue for the method proposed by Brugger et al. (2016).

Table 3. Median and inter-quartile (IQ) values of the estimated order, α, and cutoff wavenumber, k_{Th} of the low-pass filter modeling the LiDAR spatial averaging for each dataset.

	α		$k_{Th}l/(2\pi)$	
	Median	IQ Range	Median	IQ Range
SLTEST	4.898	0.358	0.176	0.008
Celina1	2.198	0.163	0.144	0.021
Celina2	4.455	0.653	0.163	0.027
Celina3	2.579	0.422	0.152	0.030

6 ~~Assessment of the correction procedure through synthetic velocity signals~~ Variability in spatial filtering with mean wind speed, turbulence intensity and sampling height

~~To better understand the importance of the filter order, α, and the cutoff frequency, f_{Th} in Eq. 10, a turbulent synthetic signal~~
450 ~~is generated, by using a sampling frequency $f_S = 20$ Hz, from the inverse Fast Fourier Transform of a Kaimal-like spectrum (Eq. 1) with $A_f = 10$ m^{2}s^{-1}, $B_f = 20$ s, and providing random phases to the various spectral contributions. The generated time series consists of 36,000 samples evenly spaced in time.~~

~~This synthetic velocity signal is convoluted in the frequency domain with Eq. 10 where the order, α, and the cutoff frequency, f_{Th}, are varied within the intervals $(\alpha, f_{Th}/f_S) = [2,5] \times [0.005, 0.25]$. The energy spectra obtained from the convolution of the synthetic signal with the various low-pass filters obtained by using the extrema of the above-mentioned ranges for α and f_{Th}/f_S are reported in Fig. 16(a), while the respective low-pass filters are depicted in Fig. 16(b). It is evident that the largest deviation from the spectrum of the original synthetic signal is associated with the minimum value of the cutoff frequency (red and cyan lines in Figs. 16(a) and (b)). On the other hand, the filter order produces a secondary effect on the spectral damping, namely a faster damping with increasing frequencies is observed with higher filter orders. To couple damping effects of both cutoff frequency and order of the low-pass filter, the percentage reduction of variance, which is calculated through Eq. 20, is reported in Fig. 16(c). This color map corroborates that the largest variability in the damping of the energy spectra occurs with variations of the cutoff frequency, while the gradient in the vertical direction, namely with variations of α, is practically negligible. Specifically, for a cutoff frequency interval ranging from 0.5% to 25% of the sampling rate, the corresponding energy reduction varies from 45% down to 5%, which is in agreement with the experimental data reported in Fig. 14(b). Therefore, for the correction of the spectral damping of the LiDAR velocity signals, the main parameter to be tuned for the correction procedure is the cutoff frequency of the low-pass filter.~~

~~We now attempt to interpret the variability in the damping of the velocity variance as a function of height observed from the experimental datasets, as it has been reported in Fig. 14(b).~~

To investigate effects of the spatial averaging on wind LiDAR measurements for different mean wind speed, turbulence intensity, and sampling height of the velocity signals, synthetic turbulent velocity spectra are generated using the spectral model of Eq. 1, while the energy damping connected with the LiDAR measuring process is estimated through Eq. 9 by using a filter order $\alpha = 3$ and $(k_{Th} l) = 0.95$, in analogy to the respective experimental values reported in Table 3.

Within the inertial sub-layer, namely for heights smaller than about 30% of the surface layer height (Marusic et al. , 2013), the mean streamwise velocity for near-neutral stability conditions can be modeled through the following logarithmic law (Monin and Obukhov , 1954; Stull , 1988):

$$U = \frac{u_\tau}{\kappa} \log\left(\frac{z}{z_0}\right), \tag{21}$$

where $\kappa = 0.41$ is the Von Kármán constant. Furthermore, we should expect a logarithmic decrease in the velocity variance with increasing wall-normal distance (Townsend , 1976), as follows:

$$\frac{\sigma^2}{u_\tau^2} = H_1 - G_1 \log\left(\frac{z}{\delta}\right), \tag{22}$$

where δ is the surface layer height, while the parameters H_1 and G_1 might be dependent on the characteristics of the specific boundary layer flow under investigation. Previous field campaigns performed at the SLTEST site have quantified them as follows: $H_1 = 2.14$ and $G_1 = 1.33$ (Marusic et al. , 2013).

According to the spectral model of Eq. 1, the velocity variance can be obtained by integrating S_u in the spectral domain, which leads to:

$$\frac{\sigma^2}{u_\tau^2} = \int_0^\infty \frac{A}{(1+Bn)^{5/3}}\, dn = \frac{3}{2}\frac{A}{B}, \tag{23}$$

where A and B vary with the sampling height.

~~To generate synthetic velocity signals throughout the boundary layer height similar to those observed from the experimental datasets, the vertical profile of B_f has been selected equal to that measured for the SLTEST dataset, which is related to the spectral peak reported with black empty circles in Fig. 11(b). Using the values of H_1, G_1 provided by Marusic et al. (2013), the logarithmic profile of variance is estimated from Eq. 21 over the height range $z/\delta \in [0.1 \quad 1]$. Finally, A_f is calculated from Eq. 22.~~

~~The convolution of the synthetic velocity signals is performed by using $\alpha = 3$ and $f_{Th} \in [0.05, \quad 0.15]$ Hz. The sampling rate is assumed equal to 20 Hz, while the total number of samples is $40{,}000$. The variance associated with the low-pass filtered velocity signals is reported as a function of height and for the various cutoff frequencies in Fig. 17(a). In agreement with the results reported in Fig. 16, a more severe damping is inferred to the synthetic velocity signals with reducing cutoff frequency. Furthermore, a lower cutoff frequency entails a more marked departure of the variance trend as a function of height from the expected logarithmic law, which also extends to higher heights.~~

~~By calculating the percentage reduction of the variance, $\epsilon_\%$, through Eq. 20, it is observed that the damping in the variance due to the LiDAR measuring process typically decreases with height until a certain asymptotic error is achieved for heights between 0.3δ-0.4δ. It is interesting that this feature singled out through the analysis of the synthetic velocity signals is very similar to that observed in Fig. 14(b) for the SLTEST dataset, for which the surface layer height, δ has been estimated between 60 m and 100 m from previous works (Hutchins and Marusic , 2007; Metzger et al. , 2007; Marusic and Hutchins , 2008). A similar trend is also observed for the dataset Celina1 even though it exhibits a larger variance error (nearly 25%). For the remaining datasets, a roughly constant percentage error has been calculated, which might correspond to the region with asymptotic $\epsilon_\%$ values observed in Fig. 17(b).~~

The first analysis is performed by varying the friction velocity, u_τ, within the range between 0.1 m s^{-1} and 0.7 m s^{-1} with a step of 0.05 m s^{-1}, while keeping fixed the sampling height $z/\delta = 0.3$ ($B = 33$ (Kaimal et al. , 1972)), and $z_0 = 10^{-4}$ m. This study aims to investigate variation in LiDAR spatial averaging for mean wind speed within the range $U \in [3, 23]$ m s^{-1}, while keeping unchanged the turbulence intensity (TI = $\sigma/U = 6.29\%$ at $z/\delta = 0.3$). The velocity standard deviation varies linearly with u_τ within the range $\sigma = [0.19, 1.35]$ m s^{-1} (Eq. 22), and the respective values of the parameter A are calculated from Eq. 23. The probe length, l, is varied from 10 m up to 100 m with a step of 10 m.

The parameter $\epsilon_\%$, which is defined in Eq. 20, is used to quantify the effects of the LiDAR spatial averaging on the variance of the wind velocity. In Fig. 13(a), it is observed that, as expected, $\epsilon_\%$ increases with increasing probe length, which indicates that the probe length is the main root cause of spatial averaging. Furthermore, it is noteworthy that for a given value of l, $\epsilon_\%$ decreases with increasing u_τ and, thus, mean wind speed, U. Indeed, by fixing the probe length, the cutoff wavenumber,

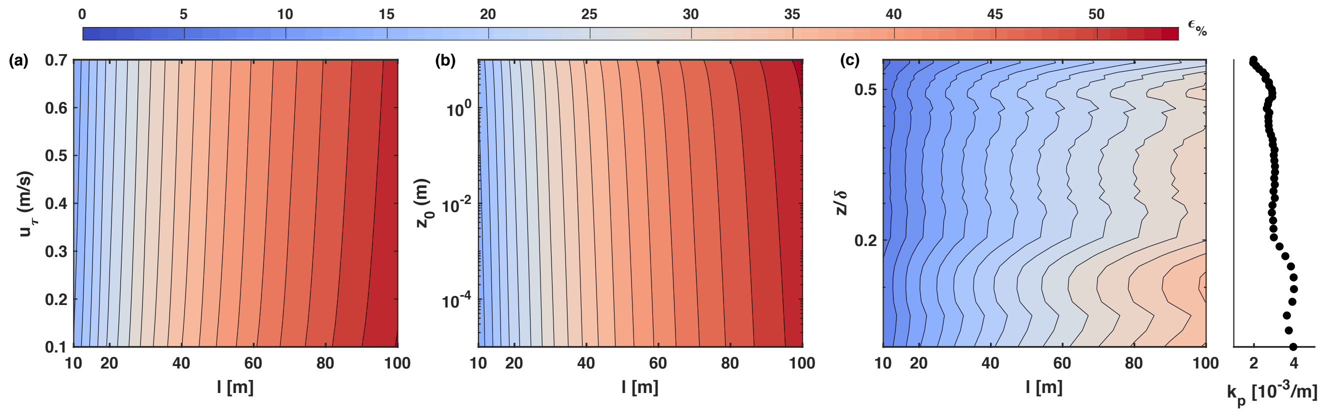

Figure 13. Variation of the percentage variance damping, $\epsilon_{\%}$ connected with the LiDAR spatial averaging for different probe lengths and wind conditions: **(a)** variability with the friction velocity, u_τ; **(b)** variability with the aerodynamic roughness length, z_0; **(c)** variability with sampling height, z. The side panel of (c) reports the vertical profile of the parameter k_p estimated for the SLTEST dataset.

k_{Th}, representing the spatial averaging is, in turn, fixed while the reduction of $\epsilon_{\%}$ with increasing U can be explained in the perspective of the Taylor frozen-turbulence hypothesis (Taylor , 1938). In other terms, with increasing U, a turbulent spectrum will shift towards lower wavenumbers (denominator in Eq. 1) and, thus, reducing the percentage of the spectral energy that is filtered for wavenumbers larger than k_{Th}.

The second test case, whose results are reported in Fig. 13(b), is performed by varying the aerodynamic roughness length within the range: $z_0 = [10^{-5}, 10]$ m, while keeping fixed u_τ= 0.5 m s^{-1}, and sampling height $z/\delta = 0.3$ (B=33). In this case, variations of z_0 affect directly the mean velocity (Eq. 21), while the velocity standard deviation is unchanged (Eq. 22). Therefore, this study can be considered as a test to investigate the effects on the LiDAR spatial averaging due to variation of the wind turbulence intensity, which might be connected to different site terrain roughness, variations of wind direction, and atmospheric stability regime. Specifically, for a fixed probe length, an increase of aerodynamic roughness length leads to a reduction of the mean velocity for a given height and friction velocity, and a shift of the turbulent spectrum towards higher wavenumbers and, in turn, enhanced effects of the spatial averaging on the LiDAR measurements.

The last case study is performed for a given wind condition, namely with $u_\tau = 0.5$ m s^{-1} and $z_0 = 10^{-4}$m, and by varying the measurement height within the range $z/\delta = [0.1, 0.6]$. The vertical variability of the parameter $B = [65,\ 228]$ has been selected equal to that measured for the SLTEST dataset, and the respective values of the wavenumber of the spectral peak, k_p, are reported in the side panel of Fig. 13(c). For each height, the velocity variance is calculated via Eq. 22 and the corresponding value of A is obtained through Eq. 23. The resulting percentage reduction of variance is plotted in Fig. 13(c). For a fixed probe length, it is observed that $\epsilon_{\%}$ generally decreases with height in a way similar to what has been observed experimentally in Fig. 11(b), and the variations of $\epsilon_{\%}$ are strongly dependent on the variations of the parameter k_p. In other words, with increasing height, the general reduction of k_p leads to a smaller percentage of the spectral energy of the velocity signal present for wavenumbers larger than k_{Th}, which is fixed once the LiDAR probe length is selected. Therefore, smaller effects of the LiDAR spatial averaging occur with increasing height for a given wind condition and probe length.

7 Conclusions

Pulsed Doppler wind LiDAR technology is gradually achieving compelling technical specifications, such as ~~range gates~~ probe lengths smaller than 20 m and sampling frequencies higher than 1 Hz, which are instrumental to investigate atmospheric turbulence with length scales typical of the inertial sub-range. However, the emission of a laser pulse over the ~~range gate~~ probe volume to measure the radial velocity entails a spatial smoothing process leading to damping on the measured variance of the velocity fluctuations. Existing methods propose to correct the effects of spatial averaging on LiDAR measurements using as input technical specifications of the used LiDAR systems, such as probe length and pulse energy distribution, which might not be available and, thus often approximated with analytical functions. According to previous works, and also confirmed through this study, existing methods have limited accuracy in correcting the LiDAR velocity fluctuations.

In this work, we have proposed to correct the measured LiDAR velocity signals by inverting the effects of a low-pass filter representing the energy damping on the velocity fluctuations due to the LiDAR measuring process. The filter characteristics, namely order and cutoff ~~frequency~~ wavenumber, are directly estimated from the spectrum of the LOS velocity under investigation. Specifically, the spectrum of the LiDAR velocity signal is fitted through the Kaimal spectral model for streamwise turbulence only for ~~frequencies~~ wavenumbers lower than a cutoff value for which the slope of the LiDAR velocity spectrum is observed to deviate from the expected $-5/3$ slope typical of the inertial sub-range. The ratio between the LiDAR and the Kaimal spectra is then fitted with the analytical expression of a low-pass filter to estimate the order and cutoff ~~frequency~~ wavenumber. An iterative procedure is proposed to estimate order and cutoff wavenumber of the low-pass filter. The modeled low-pass filter is then reverted on the LiDAR data to correct the LiDAR measurements and produce more accurate second-order statistics and spectra of the streamwise wind velocity. It is noteworthy that the Kaimal spectral model leverages surface layer similarity and, thus, the proposed method can only be used for LiDAR measurements collected within the atmospheric surface layer (ASL). Specifically for this work, we performed fixed scans with low elevation angle (less than $10°$) and azimuth angle equal to the mean wind direction to achieve good accuracy in the measurements of the streamwise velocity component, high vertical resolution ($\approx$ 1m), measurements up to the ASL height, and high sampling frequency (between 1 and 3.3 Hz).

For this study, the proposed method for correction of the LiDAR data has been applied to datasets collected during three different field campaigns and for one dataset the procedure has been assessed against simultaneous and co-located sonic anemometer data. For this case, it has been shown that the proposed procedure allows us to correct the second-order statistics of the LiDAR data to estimate a velocity variance comparable to that measured by a sonic anemometer. The compelling results obtained for the correction of the second-order statistics of LiDAR data corroborate the advantage of applying the proposed method, which does not require as input any information of the LiDAR system used, such as probe length and energy distribution over the laser pulse. In contrast to existing methods for correction of LiDAR spatial averaging, all the method parameters are directly estimated from the collected LiDAR data. However, the proposed method can only be applied for LiDAR data collected within the ASL.

~~This study has shown that it is challenging to determine a priori the cutoff frequency wavenumber and order of the low-pass filter representing the energy damping of the LiDAR measuring process for a given LiDAR system, LiDAR settings, atmospheric and wind conditions. Therefore, we rather propose to determine the parameters of the low-pass filter on a case-by-case basis by applying the proposed procedure on the LiDAR signal under investigation.~~

To better understand the role of the cutoff ~~frequency~~ wavenumber and order of the low-pass filter representing the LiDAR energy damping, further analysis has been conducted on synthetic turbulent velocity ~~signals~~ spectra. This analysis has been performed by varying mean wind speed, turbulence intensity, and sampling height. This analysis has shown that the main parameter for efficiently correct the LiDAR energy damping is the cutoff ~~frequency~~ wavenumber of the low-pass filter, which is mainly affected by the probe length, while the velocity statistics are weakly affected by the filter order. Furthermore, the results have confirmed that for a given probe length, effects of spatial averaging are enhanced with decreasing wind speed, smaller integral length scale and, thus, for a lower sampling height. ~~Subsequently, investigating effects of the LiDAR energy damping on synthetic turbulent velocity signals characterized by a logarithmic reduction of the variance with decreasing height from the ground, it has been shown that the LiDAR energy damping leads to a departure of the variance as a function of height from the expected logarithmic trend, while achieving an asymptotic percentage error with increasing heights. As expected, the energy damping is enhanced with reducing cutoff frequency of the low-pass filter and it is extend to a higher altitudes. Summarizing, the proposed procedure allows achieving efficient corrections of the second order statistics and spectra of the LiDAR measurements by inverting the effects of a low-pass filter, whose characteristics are directly estimated from the LiDAR data. However, further investigations with different LiDAR systems, LiDAR settings, such as range gate and accumulation time, and atmospheric wind conditions are needed to be able to predict a priori the correction parameters.~~

Acknowledgements. This work was supported by the National Science Foundation (NSF) CBET grant # 1705837, program manager Dr. Ronald Joslin. The authors are thankful to Eric Pardyjak, Marc Calaf and Sebastian Hoch for their support during the SLTEST experiment, and to Julie K. Lundquist for leading the XPIA field campaign.

References

Balasubramaniam, B. J.: Nature of turbulence in wall bounded flows, Ph.D. Thesis, University of Illinois at Urbana-Champaign, 2005.

Banakh, V. A. and Werner C.: Computer simulation of coherent Doppler lidar measurement of wind velocity and retrieval of turbulent wind statistics, Opt. Eng., 44(7), 071205, https://doi.org/10.1117/1.1955167, 2005.

Banerjee, T., Katul, G. G., Salesky, S. T., and Chamecki, M.: Revisiting the formulations for the longitudinal velocity variance in the unstable atmospheric surface layer, Q. J. R. Meteor. Soc., 141, 1699–1711, https://doi.org/10.1002/qj.2472, 2015.

Brugger, P., Träumner, K., Jung, C.: Evaluation of a procedure to correct spatial averaging in turbulence statistics from a Doppler lidar by comparing time series with an ultrasonic anemometer, J. Atmos. Oceanic Technol., 33(10), 2135–2144. https://doi.org/10.1175/JTECH-D-15-0136.1, 2016.

Bodini, N., Zardi, D., and Lundquist, J. K.: Three-dimensional structure of wind turbine wakes as measured by scanning lidar, Atmos. Meas. Tech., 10, 2881–2896, https://doi.org/10.5194/amt-10-2881-2017, 2017.

Carbajo Fuertes, F., Iungo, G. V., and Porté-Agel, F.: 3D turbulence measurements using three synchronous wind lidars: validation against sonic anemometry, J. Atmos. Oceanic Technol., 31, 1549-1556, https://doi.org/10.1175/JTECH-D-13-00206.1, 2014.

Cheynet, E., Jakobsen J., Snæbjörnsson J., Mann J., Courtney M., Lea G., and Svardal B.: Measurements of surface-layer turbulence in a wide Norwegian fjord using synchronized long-range Doppler wind lidars, Remote Sens., 9, 977, https://doi.org/10.3390/rs9100977, 2017.

Choukulkar, A., Brewer, W. A., Sandberg, S. P., Weickmann, A., Bonin, T. A., Hardesty, R. M., Lundquist, J. K., Delgado, R., Iungo, G. V., Ashton, R., Debnath, M., Bianco, L., Wilczak, J. M., Oncley, S., and Wolfe, D.: Evaluation of single and multiple Doppler lidar techniques to measure complex flow during the XPIA field campaign, Atmos. Meas. Tech., 10, 247-264, https://doi.org/10.5194/amt-10-247-2017, 2017.

D'Errico, J.: Inpaint nans, MATLAB Central File Exchange, 2004.

Debnath, M., Iungo, G. V., Brewer, W. A., Choukulkar, A., Delgado, R., Gunter, S., Lundquist, J. K., Schroeder, J. L., Wilczak, J. M., and Wolfe, D.: Assessment of virtual towers performed with scanning wind lidars and Ka-band radars during the XPIA experiment, Atmos. Meas. Tech., 10, 1215-1227, https://doi.org/10.5194/amt-10-1215-2017, 2017a.

Debnath, M., Iungo, G. V., Ashton, R., Brewer, W. A., Choukulkar, A., Delgado, R., Lundquist, J. K., Shaw, W. J., Wilczak, J. M., and Wolfe, D.: Vertical profiles of the 3-D wind velocity retrieved from multiple wind lidars performing triple range-height-indicator scans, Atmos. Meas. Tech., 10, 431-444, https://doi.org/10.5194/amt-10-431-2017, 2017b.

Debnath, M.: Evolution within the atmospheric boundary layer of coherent structures generated by wind turbines: LiDAR measurements and modal decomposition, Ph.D. thesis, The University of Texas at Dallas, USA, 2018.

Eberhard, W. L., Cupp, R. E., and Healy, K. R.: Doppler lidar measurement of profiles of turbulence and momentum flux, J. Atmos. Oceanic Technol., 6, 809-819, https://doi.org/10.1175/1520-0426(1989)006<0809:DLMOPO>2.0.CO;2, 1989.

Emeis, S., Harris, M., and Banta, R. M: Boundary-layer anemometry by optical remote sensing for wind energy applications, Meteorol. Z., 16, 337-347, https://doi.org/10.1127/0941-2948/2007/0225, 2007.

Foken, T., Göockede, M., Mauder, M., Mahrt, L., Amiro, W., and Munger, W.: Post-field data quality control, Handbook of Micrometeorology, Springer Netherlands, Dordrecht, 181-208, https://doi.org/10.1007/1-4020-2265-4_9, 2004.

Frehlich, R., Hannon, S. M., Henderson, S. W.: Coherent Doppler lidar measurements of wind field statistics, Bound-Lay Meteorol., 86(2), 233–256, https://doi.org/10.1023/A:1000676021745, 1998.

Frehlich, R. and Kelley, N.: Measurements of wind and turbulence profiles with scanning Doppler lidar for wind energy applications, IEEE J. Sel. Top. Appl., 1 (1), 42-47, https://doi.org/10.1109/JSTARS.2008.2001758, 2008.

Gryning, S. E., Floors, R., Peña, A., Batchvarova, E., Brümmer, B..: Weibull wind-speed distribution parameters derived from a combination of wind-Lidar and tall-mast measurements over land, coastal and marine sites, Bound-Lay. Meteorol., 159(2), 329–348, https://doi.org/10.1007/s10546-015-0113-x, 2016.

Held, D.P. and Mann, J.: Comparison of methods to derive radial wind speed from a continuous-wave coherent lidar Doppler spectrum, Atmos. Meas. Tech., 11(11), 6339-6350, https://doi.org/10.5194/amt-11-6339-2018, 2018.

Hu, R., Yang, X. I. A., and Zheng, X.: Wall-attached and wall-detached eddies in wall-bounded turbulent flows, J. Fluid Mech., 885, A30-24, https://doi.org/10.1017/jfm.2019.980, 2019.

Hutchins, N. and Marusic, I.: Evidence of very long meandering features in the logarithmic region of turbulent boundary layers, J. Fluid Mech., 579, 1-28, https://doi.org/10.1017/S0022112006003946, 2007.

Hutchins, N., Chauhan, K., Marusic, I., Monty, J., and Klewicki, J.: Towards reconciling the large-scale structure of turbulent boundary layers in the atmosphere and laboratory, Boundary-Layer Meteorol., 145, 273-306, https://doi.org/10.1007/s10546-012-9735-4, 2012.

International Electrotechnical Commission IEC 61400-1: Wind turbines-part 1: design requirements, 3 Ed., 2007.

Iungo, G. V., Wu, Y. T., and Porté-Agel, F.: Field measurements of wind turbine wakes with lidars, J. Atmos. Oceanic Technol., 30, 274-287, https://doi.org/10.1175/JTECH-D-12-00051.1 , 2013.

Kaimal, J. C., Wyngaard, J. C., Izumi, Y., and Coté, O. R.: Spectral characteristics of surface layer turbulence, Q. J. R. Meteorol. Soc., 98, 563-589, https://doi.org/10.1002/qj.49709841707, 1972.

Kaimal, J. C. and Finnigan, J. J.: Atmospheric boundary layer flows: their structure and measurement, Oxford University Press, New York, 1994.

Kristensen, L., Kirkegaard, P., and Mikkelsen T.: Determining the velocity fine structure by a laser, Technical University of Denmark, Lyngby, Denmark, 33, 2011.

Kunkel, G. J. and Marusic, I.: Study of the near-wall-turbulent region of the high-Reynolds-number boundary layer using an atmospheric flow, J. Fluid Mech., 548, 375-402, https://doi.org/10.1017/S0022112005007780, 2006.

Lindelöw, P.: Fiber based coherent lidars for remote wind sensing, Ph.D. thesis, Technical University of Denmark, Lyngby, Denmark, 2008.

Liu, H. Y., Bo, T. L., and Liang, Y. R.: The variation of large-scale structure inclination angles in high Reynolds number atmospheric surface layers, Phys. Fluids, vol. 29, 035104, https://doi.org/10.1063/1.4978803, 2017.

Lundquist, J. K., Wilczak, J. M., Ashton, R., Bianco, L., Brewer, W. A., Choukulkar, A., Clifton, A., Debnath, M., Delgado, R., Friedrich, K., Gunter, S., Hamidi, A., Iungo, G. V., Kaushik, A., Kosovic, B., Langan, P., Lass, A., Lavin, E., Lee, J. C. Y., McCaffrey, K. L., Newsom, R., Noone, D. C., Oncley, S. P., Quelet, P. T., Sandberg, S. P., Schroeder, J. L., Shaw, W. J., Sparling, L., Martin, C. S., Pe, A. S., Strobach, E., Tay, K., Vanderwende, B. J., Weickmann, A., Wolfe, D., and Worsnop, R.: Assessing state-of-the-art capabilities for probing the atmospheric boundary layer: the XPIA field campaign, B. Am. Meteorol. Soc., 98, 289-314, https://doi.org/10.1175/BAMS-D-15-00151.1, 2017.

Mann, J.: The spatial structure of neutral surface-layer atmospheric turbulence, J. Fluid Mech., 273, 141–168, https://doi.org/10.1017/S0022112094001886, 1994.

Mann, J., Cariou, P., Courtney, M. S., Parmantier, R., Mikkelsen, T. , Wagner, R. , Lindelow, P., Sjoholm, M., and Enevoldsen, K. : Comparison of 3D turbulence measurements using three staring wind lidars and a sonic anemometer, Meteorol. Z., 18(2), 135-140, https://doi.org/10.1127/0941-2948/2009/0370, 2009.

Marusic, I. and Hutchins, N.: Study of the log-layer structure in wall turbulence over a very large range of Reynolds number, Flow Turbul. Combust., 81, 115-130, https://doi.org/10.1007/s10494-007-9116-0, 2008.

Marusic, I., Monty, J. P., Hultmark, M., and Smits, A. J.: On the logarithmic region in wall turbulence, J. Fluid Mech., 716, R3, https://doi.org/10.1017/jfm.2012.511, 2013.

Meneveau, C. and Marusic, I.: Generalized logarithmic law for high-order moments in turbulent boundary layers, J. Fluid Mech., 719, 1–11, https://doi.org/10.1017/jfm.2013.61, 2013.

Metzger, M. M. and Klewicki, J. C.: A comparative study of near-wall turbulence in high and low Reynolds number boundary layers, Phys. Fluids, 13, 692-701, https://doi.org/10.1063/1.1344894, 2001.

Metzger, M. M., McKeon, B. J., and Holmes, H.: The near-neutral atmospheric surface layer: turbulence and non-stationarity, Philos. T. R. Soc. A, 135, 859-876, https://doi.org/10.1098/rsta.2006.1946, 2007.

Mikkelsen, T., Courtney, M., Antoniou, I., and Mann, J.: Wind scanner: a full-scale laser facility for wind and turbulence measurements around large wind turbines, in: Europ. Wind Energy Conf., Brussels, Belgium, 31 March - 3 April 2008, 1, 012018, 2008.

Monin, A. S. and Obukhov, A. M.: Basic laws of turbulent mixing in the surface layer of the atmosphere, Contrib. Geophys. Inst. Acad. Sci. USSR, 24, 163-187, 1954.

Ogata, K.: Modern Control Engineering, 5 Ed., Prentice Hall, Pearson, 2010.

Olesen, H.R., Larsen, S.E., and Højstrup, J.: Modelling velocity spectra in the lower part of the planetary boundary layer, Boundary-Layer Meteorol., 29(3), 285–312, https://doi.org/10.1007/BF00119794, 1984.

Panofsky, H. A. and Dutton J. A.: Atmospheric turbulence, John Wiley & Sons, New York, 1984.

Risan, A., Lund, J.A., Chang, C.Y. and Sætran, L.: Wind in complex terrain-lidar measurements for evaluation of CFD simulations, Remote Sens., 10(1), 59, https://doi.org/10.3390/rs10010059, 2018.

Sathe, A. and Mann, J.: A review of turbulence measurements using ground-based wind lidars, Atmos. Meas. Tech., 6, 3147-3167, https://doi.org/10.5194/amt-6-3147-2013, 2013.

Savitzky, A. and Golay, M. J.: Smoothing and differentiation of data by simplified least squares procedures, Anal. Chem., 36(8), 1627-1639, 1964.

Simiu, E. and Scanlan, R. H.: Wind effects on structures: fundamentals and application to design, 3 Ed., John Wiley, New York, 1996.

Sjöholm, M., Mikkelsen, T., Mann, J., Enevoldsen, K., and Courtney, M.: Spatial averaging-effects on turbulence measured by a continuous-wave coherent lidar, Meteorol. Z. , 18, 281-287, https://doi.org/10.1127/0941-2948/2009/0379, 2009.

Spuler, S.M. and Mayor, S.D.: Scanning eye-safe elastic backscatter lidar at 1.54 μm. J. Atmos. Oceanic Technol. , 22(6), 696-703, https://doi.org/10.1175/JTECH1755.1, 2005.

Stull, R. B.: An introduction to boundary layer meteorology, Springer, Dordrecht, 1988.

Taylor, G. I.: The spectrum of turbulence, P. R. Soc. London, 164, 476–490, 1938.

Townsend, A. A.: The structure of turbulent shear flow, 2nd Ed., Cambridge University Press, 1976.

To, A. C., Moore, J. R., and Glaser, S. D.: Wavelet denoising techniques with applications to experimental geophysical data, Signal Process., 89(2), 144–160, https://doi.org/10.1016/j.sigpro.2008.07.023, 2009.

Von Kármán, T.: Progress in the statistical theory of turbulence, P. Natl. Acad. Sci. USA, 34(11):530, 1948.

Weinstein, C.J.: Programs for digital signal processing, IEEE Press New York, 1979

Welch, P. D.: The use of fast Fourier transform for the estimation of power spectra: a method based on time averaging over short, modified periodograms, IEEE T. Acoust. Speech, AU-15, 70-73, https://doi.org/10.1109/TAU.1967.1161901,1967.

Worsnop, R. P., Bryan, G. H., Lundquist, J. K., and Zhang, J. A.: Using large-eddy simulations to define spectral and coherence characteristics of the hurricane boundary layer for wind-energy applications, Boundary-Layer Meteorol., 165(1), 55-86, https://doi.org/10.1007/s10546-017-0266-x, 2017.

Zhan, L., Letizia, S., and Iungo, G. V.: LiDAR measurements for an onshore wind farm: wake variability for different incoming wind speeds and atmospheric stability regimes, Wind Energy, 1-27, https://doi.org/10.1002/we.2430, 2019.

Zhan, L., Letizia, S., and Iungo, G. V.: Optimal tuning of engineering wake models through LiDAR measurements. Wind Energy Science, https://doi.org/10.5194/wes-2020-72, 1–28, 2020.